Published in final edited form as:

Nat Med. 2015 June ; 21(6): 601–609. doi:10.1038/nm.3843.

Pharmacological targeting of actin-dependent dynamin oligomerization ameliorates chronic kidney disease in diverse animal models

Mario Schiffer[1,2,*,#], **Beina Teng**[1,#], **Changkyu Gu**[3,#], **Valentina A. Shchedrina**[3], **Marina Kasaikina**[3], **Vincent A. Pham**[3], **Nils Hanke**[1], **Song Rong**[1], **Faikah Gueler**[1], **Patricia Schroder**[1,2], **Irini Tossidou**[1], **Joon-Keun Park**[1], **Lynne Staggs**[1,2], **Hermann Haller**[1,2], **Sergej Erschow**[4], **Denise Hilfiker-Kleiner**[4], **Changli Wei**[5], **Chuang Chen**[5], **Nicholas Tardi**[5], **Samy Hakroush**[6], **Martin K. Selig**[7], **Aleksandr Vasilyev**[8], **Sandra Merscher**[9], **Jochen Reiser**[5], and **Sanja Sever**[2,*]

[1]Department of Nephrology, Hannover Medical School, Hannover, Germany

[2]Mount Desert Island Biological Laboratory, Salsbury Cove, ME

[3]Department of Medicine, Harvard Medical School and Division of Nephrology, Massachusetts General Hospital, Charlestown, MA

[4]Department of Cardiology, Hannover Medical School, Hannover, Germany

[5]Department of Medicine, Rush University Medical Center, Chicago, IL

[6]Pathology Department, University Medical Center Göttingen, Göttingen, Germany

[7]Pathology Department, Massachusetts General Hospital, Charlestown, MA

[8]Department of Biomedical Sciences, NYIT COM, Old Westbury, NY

[9]Department of Medicine, Division of Nephrology and Hypertension, Leonard M. Miller School of Medicine, Miami, FL

Abstract

Dysregulation of the actin cytoskeleton in podocytes represents a common pathway in the pathogenesis of proteinuria across a spectrum of chronic kidney diseases (CKD). The GTPase dynamin has been implicated in the maintenance of cellular architecture in podocytes through its

[*]Corresponding authors: Sanja Sever, Phone: 617-724-8922; FAX: 617-726-5669, ssever@partners.org. Mario Schiffer, Phone: 49-5115324708; FAX: 49-511552366, schiffer.mario@mh-hannover.de.

[#]Equal contribution

AUTHOR CONTRIBUTIONS

M.S., H.H., J.R and S.S designed the research; B.T., C.G., V.A.S., M.K., N.H., P.S., L.S., I.T., J-K. P., S.E., D. H.–K., C.W., S. M., C.C., N.T., S.H., S.R. and F.G. performed the research. B.T., C.G., M.K., M.S., and S.S. analyzed the data. M.S., B.T., C.G. and S.S. wrote the manuscript.

COMPETING FINANCIAL INTEREST

The authors declare competing financial interests: S.S. and J.R. have pending or issued patents on novel kidney-protective therapies that have been out-licensed to Trisaq Inc. in which they have financial interest. In addition, they stand to gain royalties from their commercialization. The remaining authors report no conflicts.

direct interaction with actin. Furthermore, the propensity of dynamin to oligomerize into higher-order structures in an actin-dependent manner and to crosslink actin microfilaments into higher order structures have been correlated with increased actin polymerization and global organization of the actin cytoskeleton in the cell. We found that use of the small molecule Bis-T-23, which promotes actin-dependent dynamin oligomerization and thus increased actin polymerization in injured podocytes, was sufficient to improve renal health in diverse models of both transient kidney disease and of CKD. In particular, administration of Bis-T-23 in these renal disease models restored the normal ultrastructure of podocyte foot processes, lowered proteinuria, lowered collagen IV deposits in the mesangial matrix, diminished mesangial matrix expansion and extended lifespan. These results further establish that alterations in the actin cytoskeleton of kidney podocytes is a common hallmark of CKD, while also underscoring the significant regenerative potential of injured glomeruli and that targeting the oligomerization cycle of dynamin represents an attractive potential therapeutic target to treat CKD.

Keywords

dynamin; actin cytoskeleton; podocytes; chronic kidney diseases; proteinuria

Chronic kidney disease (CKD) affects hundreds of millions of people worldwide[1,2]. It is associated with the appearance of significant amounts of high molecular weight plasma proteins in the urine (that is, proteinuria), a symptom of a compromised glomerular filtration barrier (GFB). Renal filter selectivity is maintained by a physical, chemical, and signaling interplay between its three core cellular constituents: glomerular endothelial cells, a basement membrane and highly specialized visceral epithelial cells known as podocytes. Injury or functional impairment to any of these three components of the GFB can lead to proteinuria[3].

Podocytes are terminally differentiated cells of the glomerulus, which consist of a cell body and primary, microtubule-driven membrane extensions, as well as secondary, actin-based membrane extensions called foot processes. A number of proteins such as nephrin, CD2-associated protein (CD2AP), α-actinin 4 and inverted formin-2 (INF2) have been implicated in maintaining the podocyte's complex cytoskeletal structure and function[4–8]. In addition to genetic mutations in key genes, podocyte injury can also be driven by diabetes or hypertension[9]. Irrespective of genetic or disease-based causes, podocyte injury leads to the reorganization of the actin cytoskeleton, which underlies the loss of the actin-based foot processes[10–12], a process referred to as foot process effacement[13,14]. Sustained injury to podocytes results in molecular alterations both within the cell as well as in its extracellular environment, which ultimately causes podocyte loss and glomerular injury[12].

At present, clinical options to treat proteinuria include lowering the glomerular filtration pressure with blockers of the renin-angiotensin-aldosterone system or with immunomodulators such as cyclosporine. However, since dysregulation of the actin cytoskeleton upon podocyte injury is a highly dynamic process that involves rapid loss and re-formation of foot processes[15], it has been suggested that interventions that target actin cytoskeleton dynamics would ameliorate kidney dysfunction[16].

We and others have shown that the GTPase dynamin is essential for podocyte structure and function[17,18]. Dynamin regulates clathrin-mediated endocytosis and the actin cytoskeleton[19,20]. Dynamin has a propensity to oligomerize into higher-order structures which is promoted by lipids[21], actin filaments[22] and SH3-domain containing proteins[23]. Actin-dependent dynamin oligomerization has been implicated in regulating the actin cytoskeleton both by initiating actin polymerization through the removal of the capping protein gelsolin from the barbed ends of actin filaments and by crosslinking actin filaments[22]. Biochemical analyses using recombinant proteins and fluorescence lifetime imaging microscopy in podocytes recently showed that the small molecule Bis-T-23 promotes actin-dependent dynamin oligomerization[24,25].

Given these observations, we investigated the effects of targeting dynamin's oligomerization cycle with Bis-T-23 in whole animals. Remarkably, Bis-T-23 ameliorated or prevented proteinuria and diminished mesangial matrix expansion in diverse genetic and chronic models of glomerular disease in rodents. Our study suggests the feasibility of treating a diverse range of glomerular kidney diseases by modulating actin dynamics by targeting dynamin's oligomerization cycle.

RESULTS

Dynamin oligomerization is essential for podocyte function

We first used zebrafish as an experimental model system to test whether actin-dependent dynamin oligomerization has a physiological role in maintaining podocyte function. As recently demonstrated[26], depletion of the zebrafish homolog of dynamin, dynamin-2 (Dyn2) by a morpholino-based approach (*dnm2* MO) resulted in morphological changes in embryos such as shortened body length, upward curled tails, pericardial and yolk sac edema as compared to treatment with a scrambled control morpholino (Control MO) (Fig. 1a), and a significant difference in survivorship (Fig. 1b).

The selectivity of the zebrafish glomeruli for proper protein filtration is assessed by measuring the fluorescence intensity of transgenically overexpressed eGFP-tagged vitamin D-binding protein (eGFP-DBP) in the retinal blood vessel of the fish eye as a measure of circulating eGFP-DBP[27]. A decrease in circulating eGFP-DBP is typically accompanied by foot process effacement and appearance of eGFP-DBP-mediated fluorescence in the tank water, indicative of a compromised GFB in the manipulated fish[28,29]. We used this physiological screen in our study and compared to Control MO-treated fish, *dnm2* MO-treated embryos exhibited foot process effacement (Fig. 1c) and a significant decrease in circulating eGFP-DBP (Fig. 1d). Although the zebrafish genome contains the genes *dnm2*, *dnm1-like* and *dnm1*, which encode for three different dynamin isoforms, these observed phenotypes can be attributed to a specific depletion of *dnm2* as *dnm2* MO treatment did not alter *dnm1* or *dnm1-like* mRNA expression (Supplementary Fig. 1a), while also suggesting a lack of compensation for depletion of *dnm2* expression.

To test whether the kidney phenotypes were due to loss of dynamin's role in regulating the actin cytoskeleton, we performed cross-species rescue experiments in zebrafish using rat and human isoforms and the human isoform with distinct functional mutations: rat Dyn2; human

dynamin-1 (Dyn1); human dynamin-1 E/K ($Dyn1^{E/K}$), a mutant with increased actin-dependent oligomerization[22,25]; human dynamin-1 K/E ($Dyn1^{K/E}$), a mutant with decreased actin-dependent oligomerization[22,25]; and human dynamin-1 I690K ($Dyn1^{I690K}$), an oligomerization-incompetent mutant[30] (Fig. 1d–f). Expression of rat Dyn2 or human Dyn1 in *dnm2* MO-treated fish rescued the global morphological changes (data not shown) and resulted in circulating eGFP-DBP levels comparable to control fish (Fig. 1d). Recovery of normal eGFP-DBP levels was also observed when the *dnm2* MO-treated fish co-expressed $Dyn1^{E/K}$, but not when they expressed $Dyn1^{K/E}$ or $Dyn1^{I690K}$ (Fig. 1d). Finally, expression of $Dyn1^{K/E}$ or $Dyn1^{I690K}$ was in themselves sufficient to lower circulating eGFP-DBP levels (Fig. 1d), indicating these proteins function as dominant negatives, consistent with their effects on the actin cytoskeleton in mammalian podocytes (Supplementary Fig. 1b–e)[22]. Together, these results show that actin-dependent dynamin oligomerization is essential for proper GFB function.

Dynamin can be therapeutically targeted by Bis-T-23

We next assessed the effect of Bis-T-23 on circulating eGFP-DBP levels in different genetic backgrounds (Fig. 1d). We first verified that Bis-T-23 promoted oligomerization of zebrafish Dyn2, as shown by an increase in GTPase activity (Supplementary Fig. 2a) and by the presence of dynamin oligomers in the pellet fraction after high-speed centrifugation (Supplementary Fig. 2b). This is expected given the high percent of homology between mammalian and fish Dyn2 (Supplementary Fig. 2c). Administration of Bis-T-23 had no effect on circulating eGFP-DBP levels in wild-type animals (Supplementary Fig. 2d), control MO- or *dnm2* MO-treated fish (Fig. 1d). Moreover, Bis-T-23 did not significantly improve the rescue of eGFP-DBP levels in *dnm2* MO-treated fish co-expressing Dyn1 or $Dyn1^{E/K}$ (Fig. 1d). We conclude that Bis-T-23 has no effect in animals that lack dynamin altogether or in animals expressing functional dynamin. In contrast, Bis-T-23 restored circulating eGFP-DBP to control levels in zebrafish expressing dominant negative $Dyn1^{K/E}$ or $Dyn1^{I690K}$, but not if endogenous Dyn2 was also lacking (Fig. 1d). Bis-T-23 also has no influence of survivorship of fish treated with *dyn2* MO and co-expressing $Dyn1^{K/E}$ or $Dyn1^{I690K}$ compared to these fish treated with DMSO (Supplementary Fig. 2e,f). The inability of Bis-T-23 to restore eGFP-DBP levels in the absence of endogenous dynamin provides genetic evidence that this compound directly targets dynamin. Together, these findings suggest that Bis-T-23 targets actin-dependent dynamin oligomerization in podocytes to promote proper GFB function.

We also found greater fluorescence staining in the tail of Bis-T-23-treated wild-type fish compared to DMSO treated fish (Supplementary Fig. 2g), suggesting the compound results in thicker actin filaments. These findings are consistent with the ability of dynamin oligomerization to increase actin polymerization and to crosslink actin filaments[22,25]. Moreover, Bis-T-23 increased the number of focal adhesions (FAs) and stress fibers in cultured podocytes (Supplementary Fig. 1c–e), phenocopying the expression of the gain-of-function mutant $Dyn1^{E/K}$ in these cells (Supplementary Fig. 1c–e)[22].

Dynamin oligomerization attenuates transient proteinuria

Pharmacokinetic studies showed that Bis-T-23 is rapidly absorbed into the bloodstream of mice after intraperitoneal injection into the body cavity, where it reaches its highest concentration within 15 min (Fig. 2a and Supplementary Fig. 3a). Administration of several different concentrations of Bis-T-23 to wild type, healthy mice did not induce transient proteinuria as determined by urine albumin/creatinine ratios (ACRs) measured from spotted urine (known as ACR analysis on spot urine) (Fig. 2b), late onset lasting proteinuria (Supplementary Fig. 3b), or any other obvious toxic effects (for example, discomfort, lack of movement, ruffled fur, physiological abnormalities or signs of toxicity in the liver (data not shown)). In addition, prolonged administration of Bis-T-23 did not produce any alterations in the glomerular filtration rate, as measured by inulin clearance (Fig. 2c), urinary output (Fig. 2d), renal plasma flow as measured by para-aminohippurate clearance (Fig. 2e), blood pressure (Fig. 2f) or blood urea (BU) levels (Supplementary Fig. 3c), demonstrating that Bis-T-23 did not induce nephrotoxic effects.

We next examined the effects of Bis-T-23 on transient proteinuria induced in mice by the administration of lipopolysaccharides (LPS) at time zero and again twenty four hours later. Bis-T-23 or DMSO (or no treatment) was then given twenty fours after the second LPS injection and ACR analysis on spot urine showed significantly lower proteinuria in the Bis-T-23 treatment group compared to untreated LPS-injected mice or those treated with DMSO, with the most pronounced effect occurring between 2 and 4 hours after administration of the compound (Fig. 2g). The timing of this effect was consistent with the timing of Bis-T-23 clearance from the blood (Fig. 2a), and was not a consequence of alterations in BU levels (Supplementary Fig. 3c).

It has been suggested that LPS-induced transient proteinuria is partially due to proteolytic degradation of dynamin by cytoplasmic cathepsin L (CatL)[17,31]. As reported, administration of LPS to cultured mouse podocytes leads to the loss of stress fibers and FAs[17], which was then reversed by either Bis-T-23 or the CatL inhibitor, E64 (Supplementary Fig. 4a,b). Notably, Bis-T-23 restored dynamin but not synaptopodin or RhoA levels in LPS-treated podocytes, whereas E64 restored all three proteins (Supplementary Fig. 4c). These results show that Bis-T-23 specifically affects dynamin, and they suggest that the beneficial effects of Bis-T-23 on proteinuria can be explained in whole, or in part, by the assembly of oligomerized dynamin (Supplementary Fig. 4d).

We also examined the effect of Bis-T-23 on puromycin aminonucleoside-induced nephrosis (PAN model)[32]. We injected rats with puromycin aminonucleoside on day 0, and on day 12, when proteinuria was high, we injected Bis-T-23. Bis-T-23 significantly reduced proteinuria on days 18 and 24 (Fig. 2h). Together, these data strongly suggest that pharmacological induction of dynamin oligomerization can ameliorate transient proteinuria in rodents.

Dynamin oligomerization protects podocytes from injury

To further test our hypothesis that dynamin oligomerization exhibits a protective role during podocyte injury, we generated transgenic mice expressing human Dyn1^{R725A} mutant in podocytes. The R725A mutation is situated within the GTPase effector domain (GED) (Fig.

3a), and enhances dynamin's propensity to oligomerize [33]. Homozygous *DNM1*$^{R725A/R725A}$ animals (herein referred to as DYN1^{R725A} transgenic mice) expressed human Dyn1^{R725A} mutant from a doxycycline-inducible, podocin-specific promoter (Fig. 3a). We detected the presence of mRNA encoding for Dyn1^{R725A} in glomerular extracts within one week of feeding animals with doxycycline (Fig. 3b).

While DYN1^{R725A} mice exhibited normal global glomerular morphology (Fig. 3c), the length of the foot processes were roughly double compared to control animals (podocin-Cre-only transgenic mice) (Fig. 3c,d). The ability of Dyn1^{R725A} to lengthen foot processes is consistent with its effect on FAs and stress fibers in cultured mouse podocytes (Supplementary Fig. 1c–e). In addition, DYN1^{R725A} mice were significantly protected from LPS-induced proteinuria (Fig. 3e). In these animals, LPS did not induce the transient foot process effacement observed in control animals or in DYN1^{R725A} transgenic animals in the absence of doxycycline (Fig. 3f). Together with the Bis-T-23 experiments above, these findings show that dynamin oligomerization plays a protective role in LPS-induced transient proteinuria.

To directly test our hypothesis that Bis-T-23 was acting by targeting the actin cytoskeleton in podocytes, we next examined the effect of Bis-T-23 on proteinuria using a genetic model of CKD. A point mutation, K256E, in the α-actinin 4 protein, causes hyper-bundling of actin filaments in podocytes and focal segmental glomerulosclerosis in homozygous *Actn4*$^{K256E/K256E}$ animals (herein referred to as ACTN4 mice)[8,34]. In this model, a single dose of Bis-T-23 caused a transient reduction of proteinuria compared to mice without treatment or with DMSO (Fig. 4a), which correlated with the ability of Bis-T-23 to induce FAs and stress fibers in podocytes from ACTN4 mice[35] (Supplementary Fig. 5a,b). In a complementary approach, we expressed the Dyn1^{R725A} mutant transiently in podocytes using tail vein injection of DNA encoding for mutant protein, which we previously showed induces podocyte-specific expression[17]. Although ACTN4 mice exhibited different levels of proteinuria at baseline (Fig. 4b)[34], expression of Dyn1^{R725A} resulted in markedly reduced proteinuria compared to baseline values in every case (Fig. 4b,c), occasionally reducing proteinuria to those seen in control animals (Fig. 4c). These results show that targeting dynamin oligomerization by two independent means (use of Bis-T-23 or expression of Dyn1^{R725A}) is able to ameliorate proteinuria by altering actin dynamics.

Dynamin oligomerization ameliorates CKD in diverse models

We next tested whether targeting dynamin oligomerization using Bis-T-23 is able to reverse proteinuria in diverse genetic models of CKD. Homozygous CD2AP knockout mice (*Cd2ap*$^{-/-}$)[7], herein referred to as CD2AP^{KO} mice, are born with intact slit diaphragms but the animals become mildly proteinuric by postnatal day 18 (P18) due to a defect in signaling at the slit diaphragm (Fig. 4d)[36]. Strikingly, administration of Bis-T-23 for six consecutive days almost completely prevented the onset of high-level proteinuria in the CD2AP^{KO} mice (Fig. 4d,e), and this correlated with substantial restoration of the actin cytoskeleton in cultured CD2AP^{KO} podocytes (Supplementary Fig. 5c,d). Furthermore, Bis-T-23 significantly extended the lifespans of CD2AP^{KO} mice (Fig. 4f), suggesting that protection against high-level proteinuria affects the course of the disease and subsequent mortality.

Mice with a genetic deletion of the gene encoding PKCε (*Prkce*$^{-/-}$)[37], herein referred to as PKCε^{KO} mice, are defective in multiple signaling pathways that regulate actin cytoskeleton[38], develop proteinuria and visible signs of glomerular injury by ~12 weeks of age (Fig. 5a and Supplementary Fig. 6). A single dose of Bis-T-23 administered daily to PKCε^{KO} mice not only prevented the progression of proteinuria but also significantly lowered proteinuria over the course of 8 days compared to untreated mice or those treated with DMSO (Fig. 5a). Importantly, these animals also exhibited a striking lower number of glomeruli with moderate to advanced mesangial expansion compared to untreated or DMSO-treated mice (Fig. 5b,c) and contained wild-type appearing foot processes compared to DMSO-treated mice (Fig. 5d).

The effects of Bis-T-23 on proteinuria and morphology of foot processes correlated with the ability of Bis-T-23 to restore the normal global organization of the actin cytoskeleton in cultured podocytes from PKCε^{KO} mice. Loss of PKCε results in a profound loss of FAs and stress fibers, which are almost completely rescued by re-expression of PKCε, but not a protein harboring a K437A mutation (PKCε^{K437A}), which renders the enzyme kinetically dead (Supplementary Fig. 7a–c). **C**ell extracts generated from podocytes from PKCε^{KO} mice were defective in actin polymerization, depolymerization and TGFβ– and PMA- (phorbol 12-myristate 13-acetate, a PKC activator) induced cycles of cofilin-1 (cfl1, actin-binding protein which disassembles actin filaments) phosphorylation (Supplementary Fig. 7d–g). Expression of Dyn1$^{E/K}$ or addition of Bis-T-23, but not expression of Dyn1$^{K/E}$, restored FAs and cell size, increased actin polymerization without affecting actin filament depolymerization (Supplementary Fig. 7a–c,h,i), or impairing the phosphorylation cycle of cofilin-1 (Supplementary Fig. 7j). Together, these results strongly argue that Bis-T-23 reverses proteinuria in PKCε^{KO} mice by targeting the actin cytoskeleton even when multiple regulatory pathways have been affected.

To further examine how broadly Bis-T-23 can ameliorate proteinuria, we examined different genetic models of podocyte injury in zebrafish. In addition to knocking down the expression of PKCε (with *prkce* MO) and CD2AP (with *cd2ap* MO), we also knocked down the expression of inverted formin-2 (with *inf2* MO), an actin binding protein that severs actin filaments and accelerates their polymerization and depolymerization[39], and nephrin (with *nphs1* MO), a structural slit diaphragm protein[40]. The lifespans of the fish treated with *cd2ap* MO, *prkce* MO and *inf2* MO were all shortened compared to fish treated with a control MO (Supplementary Fig. 8a). Comparable to what was observed earlier in *dnm2* MO-treated fish, *prkce* MO-treated fish exhibited shortened body length, upward curled tails, and pericardial and yolk sac edema compared to control MO-treated fish (Supplementary Fig. 8b,c). In accordance with impaired kidney function, there was a marked lowering of the level of circulating eGFP-DBP in all four models compared to control MO-treated fish (Supplementary Fig. 8d).

Injection of Bis-T-23 was associated with significantly higher circulating eGFP-DBP in *cd2ap* MO-, *prkce* MO- and *inf2* MO-treated fish compared to DMSO treatment of these fish, but not in *nphs1* MO-treated fish compared to DMSO treatment (Supplementary Fig. 8d). Electron microscopy confirmed that proteinuria in *prkce* MO-treated fish was due to foot process effacement, whereas the addition of Bis-T-23 was associated with normal foot

process morphology (Supplementary Fig. 8e). Concomitant with its effect on proteinuria, Bis-T-23 increased the lifespans of fish treated with *cd2ap* MO, *prkce* MO and *inf2* MO, but not *nphs1* MO compared to DMSO treatment (Supplementary Fig. 8f–i). Therefore, while Bis-T-23 reversed podocyte injury driven by disruption of multiple signaling pathways, it was unable to reverse injury due to loss of a structural protein such as nephrin.

Finally, we tested the effect of targeting the actin cytoskeleton via dynamin oligomerization in acquired kidney injury due to diabetes. Diabetes was induced in the majority of mice within 2–3 days after a single high dose of streptozotocin (STZ)[41]. Over a period of 16 weeks the mice developed proteinuria (Fig. 6a). Administration of Bis-T-23, but not DMSO, resulted in lower proteinuria after 8 consecutive days of administration (Fig. 6a). In addition, Bis-T-23, as compared to DMSO, led to improved glomerular histology with less mesangial matrix accumulation, as determined by Periodic Acid-Schiff (PAS) staining, Toluidine blue staining of semi-thin sections, and transmission electron microscopy (Fig. 6b). Furthermore, Bis-T-23 treatment correlated with less expression of collagen IV in sclerotic lesions compared to DMSO-treated diabetic mice (Fig. 6b,c). We observed no effect of Bis-T-23 on the level of glucose in the blood (Fig. 6d). Together, these findings not only show the ability of Bis-T-23 to lower proteinuria induced by diabetes, but further underscore the positive effect of Bis-T-23 on glomerular morphology as evidenced by reduced signs of mesangial matrix expansion.

DISCUSSION

Podocyte injury accompanied by a dysregulated actin cytoskeleton is observed in almost all cases of proteinuric CKD. In this report, we show the feasibility of targeting the actin cytoskeleton through dynamin and that this strategy has therapeutic potential to combat CKD. Given the role of the cytoskeleton in a number of diverse diseases such as cancer and CKD, earmarking the cytoskeleton as a therapeutic target has been suggested previously[16,42]. Indeed, compounds aimed at microtubule dynamics are among the most successful anticancer therapies available[43]. When it comes to targeting the actin cytoskeleton, actin filament-specific therapeutics has never been tested in humans. Our insight that the GTPase dynamin directly regulates actin dynamics via its oligomerization cycle[22,25] suggested that it might be possible to target the actin cytoskeleton using dynamin as a proxy. Using the small molecule Bis-T-23, which promotes actin-dependent dynamin oligomerization[25], we now report successful targeting of the podocyte actin cytoskeleton in diverse animal models of CKD.

Using a combination of diverse dynamin mutants, experimental organisms and Bis-T-23 we establish the physiological role of dynamin oligomerization in regulating actin cytoskeleton. Morpholino-mediated knockdown of *dnm2* in zebrafish decreased circulating eGFP-DBP, a phenotype that was rescued by presence of wild-type Dyn2 but not by $Dyn1^{K/E}$ (impaired in actin binding) or Dyn^{I690K} (impaired in oligomerization). Overexpression of both mutants induced proteinuria by forming hetero-oligomers with endogenous dynamin[22,30,44]. This effect was reversed by Bis-T-23, but only in the presence of endogenous zebrafish Dyn2, providing direct evidence that Bis-T-23 promotes actin-dependent dynamin oligomerization in the kidney. In a complementary approach, we showed that $DYN1^{R725A}$ mice exhibited

unusually long foot processes, further providing evidence that dynamin oligomerization regulates actin dynamics in podocytes. Accordingly, DYN1^{R725A} mice were protected from LPS-induced proteinuria. In further support of Bis-T-23 targeting the actin cytoskeleton, this compound transiently lowered proteinuria in ACTN4 mice.

The ability of Bis-T-23 to ameliorate proteinuria and improve glomerular morphology in extremely diverse models of transient kidney disease (LPS and PAN-induced proteinuria) and CKD (ACTN4, PKCε^{KO}, CD2AP^{KO} and STZ-induced diabetes) further validates the idea that actin dysregulation is a common downstream manifestation of podocyte injury. While actin cytoskeleton dynamics is classically linked to foot process effacement and reformation, it has been suggested that active remodeling of cortical actin regulates the spatiotemporal organization of cell surface molecules[45]. Given the unique characteristics of dynamin as a regulatory GTPase that can bind membranes and directly crosslink actin filaments and stimulate actin polymerization, we suggest that dynamin oligomerization can amend injured podocytes by modulating their morphology (that is, reformation of proper foot processes) and signaling properties. Signaling can take the form of positive crosstalk between podocytes, endothelial cells, mesangial cells, and maybe even progenitor cells of the glomerulus[46–48]. Supporting this rationale, it has been shown that alterations in the signaling within podocytes initiated proteinuria via crosstalk between podocytes and endothelial cells, and that proteinuria preceded foot processes effacement[49]. Further supporting a role for actin dynamics beyond morphological changes within foot processes, Bis-T-23 prevented and reversed early signs of glomerular injury. Together our study suggests that targeting dynamin's oligomerization cycle might break a vicious cycle of actin dysregulation triggered by missing or defective upstream signals.

In light of dynamin's central role in regulating podocyte actin dynamics, our study suggests that dynamin oligomerization represents a viable target in treating CKD. Currently no specific therapeutic option exists for proteinuria in CKD in general, and no specific treatment option exists for genetic forms of focal segmental glomerulosclerosis in particular. Given that the majority of podocyte injury in CKD can be traced back to the dysregulation of actin[10–12], the direct targeting of actin cytoskeleton dynamics in podocytes appears to be an attractive therapeutic approach for human proteinuric kidney diseases.

METHODS

General experimental approaches

No samples, mice or data points were excluded from the reported analysis. Samples were not randomized to experimental groups. All analyses were performed unblinded except the following: Measurement of intensity of circulating eGFP-DBP in the retinal vessel plexus of the fish eye and record of survivorship for all reported analyses, quantification of mesangial matrix expansion in glomeruli isolated from PKCε^{KO} mice, semi-quantitative analysis of Collagen IV staining in STZ experiments, and the length of the foot processes in DYN1^{R725A} animals.

Materials, antibodies, and standard techniques

Bis-T-23 (2-cyano-*N*-{3-[2-cyano-3-(3,4,5-trihydroxyphenyl) acryloylamino]propyl}-3-(3,4,5 trihydroxyphenyl)acrylamide) (Aberjona Laboratories, Inc., Beverly, MA) was prepared as 30 mM stock solutions in DMSO and stored frozen. The required amounts were added to the reaction vessel, achieving final DMSO concentrations of 1% or less. DMSO and GTP were from Sigma-Aldrich (St. Louis, MO). DMSO was used as a control vehicle (0.1% - 1%) in all experiments. All other reagents were of analytical reagent grade or better. Human Dyn1 and rat Dyn2 were expressed using BacPAK baculovirus expression systems (Clontech, Mountain View, CA) in Sf21 insect cells. All dynamins, with the exception of zebrafish Dyn2, were purified using the GST-SH3 domain of amphiphysin II, as described[50]. The zebrafish Dyn2 cDNA (clone ID:7437981, GeneBank Accession: BC097134) was purchased from Open Biosystems (Lafayette, CO) and cloned into the mammalian expression vector, pcDNA3.1 (Invitrogen, Carlsbad, CA), as a 6xHis tagged fusion construct. His-tagged protein was purified using HisPur Cobalt resin (Thermo Scientific, Waltham, MA) from the protein lysate of HeLa cells. The GTPase assays were performed as described[51], in a buffer containing 20 mM HEPES-KOH pH=7.5, 100 mM KCl, 2 mM $MgCl_2$, 1 mM DTT, and Malachite Green Stock Solution (1 mM Malachite Green, 10 mM ammonium molybdate in 1N HCl). Pelleting of Dyn^{OLIGO} upon high-speed centrifugation was performed in a buffer containing 20 mM HEPES, 1 mM $MgCl_2$, 1 mM EGTA (pH=7.5), and 150 mM NaCl.

Antibodies—anti-Dyn (Hudy 1, EMD Millipore, Billerica, MA; Cat#: 05-319, mouse monoclonal, 1:1000 for Western blot); anti-Dyn1 (Enzo Life Sciences, Farmingdale, NY; VAM-SV041, mouse monoclonal, 1:1000 for Western blot); anti-Dyn2 (Santa Cruz Biotechnology, Santa Cruz, CA; Cat#: sc-6400, goat polyclonal, 1:200 for Western blot); anti-paxillin (Millipore, Temecula, CA; Cat#: 04-581, rabbit monoclonal, 1:250 for Immunofluorescence); Rhodamine-phalloidin (Invitrogen, Darmstadt, Germany; Cat#: R415, 1:250 for Immunofluorescence); anti-nephrin (Santa Cruz Biotechnology, Santa Cruz, CA; Cat#: sc-28192, rabbit polyclonal, 1:200 for Western blot); anti-podocalyxin (R&D, Minneapolis, MN; Cat#: AF1556, goat-polyclonal, 1:1000 for Western blot); anti-synaptopodin (Santa Cruz Biotechnology, Santa Cruz, CA; Cat#: sc-21536, goat-polyclonal, 1:200 for Western blot); anti-podocin (Santa Cruz Biotechnology, Santa Cruz, CA; Cat#: sc-21009, rabbit polyclonal, 1:200 for Western blot); anti-Rho A (Santa Cruz Biotechnology, Santa Cruz, CA; Cat#: sc-418, mouse monoclonal, 1:200 for Western blot); anti-β-tubulin (Sigma-Aldrich, St. Luis, MO; Cat#: T8328, mouse monoclonal, 1:1000 for Western blot); anti-GAPDH (abcam, Cambridge, MA; ab8245, mouse monoclonal, 1:5000 for Western blot); anti-His tag (Qiagen, Hilden, Germany; Cat#: 34460, penta-His conjugated kit); anti-Phospho-Cofilin (Santa Cruz Biotechnology, Santa Cruz, CA; Cat#:sc12912-R, rabbit polyclonal, 1:1000 for Western blot); and anti-Cofilin-1 (Cytoskeleton Inc., Denver, CO; Cat#:ACFL02-B, 1:1000 for Western blot).

In vitro experiments

Dynamin cleavage by CatL—Dyn1 (1μM) was diluted in a buffer (pH 5.0) containing 200 mM NaCl, 10 mM HEPES pH 7.0, 2 mM EGTA, 1 mM $MgCl_2$, and 1 mM DTT. When indicated, DMSO (2.5 %) or indicated concentration of Bis-T-23 was added. Mixtures were

incubated for 20 min at room temperature. As a positive control, GTPγS (1 mM) was added and allowed to bind to Dyn1 for 10 min on ice. The reaction was initiated by addition of 2 μl of purified CatL (specific activity > 0.5 U/mg of protein from Sigma-Aldrich, St. Luis, MO) and placement of samples in 37°C water bath for 30 minutes. Total assay volume was 20 μl. The reaction was terminated with addition of E 64 inhibitor (Sigma-Aldrich, St. Luis, MO) and sample buffer. 10 μl of the samples was run on 10% SDS-PAGE, followed by silver staining (Thermo Scientific).

Actin and paxillin staining and quantification—Cells were stained anti-paxillin antibody and rhodamine-phalloidin. Images were captured with a Zeiss LSM 5 PASCAL laser scanning microscope and a 40x objective. For quantification of actin, cells were imaged with above microscope using a fixed exposure for phalloidin. The intensity of the actin staining was measured from whole cells by Image J (v1.47m) software. Total fluorescence from control (DMSO-treated or wild-type Dyn1 infected) cells and mutant Dyn1-infected and/or drug-treated cells was analyzed separately, with staining intensity normalized to the control cells. The experiment was repeated at least three times. Number of FAs was determined by integrated morphometry analysis performed using Image J (v1.47m) on thresholded images to select classified objects of a size range of >1 pixels as FAs, based on anti-paxillin staining. The analyzed particles command was used to measure number of FAs. When indicated, data were further analyzed using GraphPad Prism (v 4.03) for Windows (GraphPad Software, San Diego, CA) to perform statistical analysis using two-tailed unpaired *t*-tests. Based on this analysis, $*P \leq 0.05$, $**P \leq 0.01$, $***P \leq 0.001$ were considered statistically significant, and $P > 0.05$ was considered not significant.

Pyrene actin polymerization assay—The differentiated podocytes were lysed with G-buffer (5mM Tris-HCl pH 8.0, 0.2 mM $CaCl_2$, 200 μM ATP). Protein concentration was measured with BCA reagent. G-actin stock was prepared by adding 225 μl of ice cold G-buffer to 0.1 mg pyrene actin to get a final concentration of 0.4 mg/ml and mixing well and leaving on ice for 1 h to depolymerize actin oligomers. The G-actin stock was centrifuged at 14,000 rpm at 4°C for 30 min and the supernatant was transferred into a new tube on ice. 200 μl G-actin stock was added to each well of a 96-well plate. The fluorescence intensity of pyrene actin was measured in a TECAN plate reader with extinction of 360 nm and emission of 420 nm. Base line was established by measuring the fluorescence intensity for 5 min. At least 30 μg podocyte lysate with 20 μl actin polymerization buffer (500 mM KCl, 20 mM $MgCl_2$, 10 mM ATP) was added to each well and the increased fluorescence intensity was measured every 60 sec for 50 min.

Pyrene actin depolymerization assay—For the depolymerization assay, pyrene F-actin was prepared by quickly thawing frozen actin on ice. Pyrene actin was diluted by adding G-buffer to a final concentration of 1 mg/ml. Actin was polymerized after adding 10x actin polymerization buffer (0.25x final strength) and incubated at RT for 1 h. 200 μl F-actin stock was added in each well of a 96-well plate. After measuring the base line of fluorescence intensity, the podocyte lysate was added to each well and the decreased fluorescence intensity was measured every 60 sec for 50 min.

Cell culture and immunofluorescence

Wild-type and all other mouse podocyte cell lines were grown as described[52]. Immortalized PKCε^{KO} podocytes[53], immortalized ACTN4 podocytes[35], and immortalized CD2AP^{KO} podocytes[54] have previously been described. Adenoviral infections of cultured podocytes were performed as described[17].

Cultured podocytes were stained with anti-paxillin antibody and rhodamine-phalloidin. Images were captured with a Zeiss LSM 5 PASCAL laser scanning microscope under a 40x objective lens. For quantification of actin, cells were imaged with the aforementioned microscope using a fixed exposure for phalloidin. The intensity of the actin staining was measured from whole cells by Image J (v1.47m) software. Total fluorescence from control (DMSO-treated or wild-type Dyn1 infected) cells and mutant Dyn1-infected and/or drug-treated cells was analyzed separately, with staining intensity normalized to the control cells. Number of focal adhesions was determined by integrated morphometry analysis performed using Image J (v1.47m) on thresholded images to select classified objects of sizes >1 pixels as focal adhesions, based on anti-paxillin staining. The analyzed particles command was used to measure the number of focal adhesions. Data were plotted as mean ± SD from at least three independent experiments and statistical significance was determined using unpaired *t*-test calculated using Prism software (GraphPad, La Jolla, CA).

Experiments using zebrafish

Zebrafish stains: wild-type AB (ZIRC, Eugene, OR), Tg (l-fabp:DBP-EGFP), and Tg (L-FABP:DBP-EGFP)[55]. All strains were grown and mated at 28.5°C and embryos were kept and handled in standard E3 solution as previously described[28]. Morpholinos were injected in one- to four-stage fertilized eggs using a Nanoject II injection device (Drummond Scientific, Broomall, PA).

Morpholino injection—The following splice donor morpholinos were designed and ordered from GeneTools (Philomath, OR):

Control MO: 5′-CCTCTTACCTCAGTTACAATTTATA-3′,

prkce MO: 5′-TCAGCAGACCGTTAAAAACCACCAT-3′,

cd2ap MO: 5′-CATACTCCACCACCACCTCAACCAT-3′,

inf2 MO: 5′-AGAGTTAAGGTCACACTTGCCTTGT-3′

nphs1 MO: 5′-CGCTGTCCATTACCTTTCAGGCTCC-3′

dnm2 MO: 5′-CAACCCCACTGCTCTCACCGGATCT-3′

Morpholino injections were carried out with concentrations ranging from 25 to 250 μM, with an injection volume of 4.6 nL in 100 mM KCl and 0.1% phenol red. Embryos were monitored for the development of the phenotype until 120 hours post-fertilization. The phenotype was scored P1 to P4, based on the amount of edema present in the yolk sac or the presence of pericardial effusion. Rescue experiments were performed using mRNA injections expressing rat Dyn2 or human Dyn1, Dyn1$^{E/K}$, Dyn1$^{K/E}$, and Dyn1^{I690K}. Rescue plasmids were linearized and transcribed using the T7 mMessage Machine kit (Ambion,

Grand Island, NY). The integrity and concentration of mRNA was determined by lab-on-chip technology in a bioanalyzer (Agilent Technologies, Santa Clara, CA).

Bis-T-23-injections—For Bis-T-23 rescue studies, dechorionated embryos were anesthetized at 48 hours post-fertilization with a 1:20 to 1:100 dilution of 4 mg/ml Tricaine (MESAB: ethyl-3 aminobenzoate, methanesulfonate acid salt 1% Na_2HPO_4, pH 7.0, Sigma-Aldrich) and placed in a 1.2% agarose mold for injection. The cardinal veins of the embryos were then injected with either 4.6 nl 20% DMSO in saline or 4.6 nl of 0.2 mg/ml Bis-T-23 diluted in DMSO and saline.

Eye Assay—Fluorescence intensity of retinal blood vessels was measured in Tg (L-FABP:DBP-EGFP) zebrafish at 96 hours post morpholino injection[27]. The eye assay was performed in order to measure the accumulation of high molecular weight green fluorescent proteins in circulation in the fish as an indirect measure of proteinuria, as previously described[28,56]. At 48 hours post morpholino injection, the remaining chorions were manually removed from all of the embryos.

Image analysis—For eye assay measurements, zebrafish larvae were transferred into individual wells of a 96-well plate (Fisher Scientific, Pittsburgh, PA). The fish were anesthetized with Tricaine. Images of live fish were generated using Axiovert 200 inverted microscope (Zeiss, Thornwood, NY) connected to an AxioCam MRm charge-coupled device camera. Images were taken with fixed exposure times and gain using the Axio Vision release 4.5 SP1 software package. The maximum fluorescence intensities of each pupil image were measured using ImageJ software application (NIH, Bethesda, MD) and reported in relative units of brightness. Data collection was performed in a blind manner. The level of GFP-intensity was reported for each measured animal (at least 50 animals were measured for each condition). No data points have been excluded. Median intensity in each group has been calculated and significance was determined using unpaired *t*-test calculated using Prism software (GraphPad, La Jolla, CA).

RNA isolation from zebrafish embryos—Messenger RNA was extracted from zebrafish embryos 72 hours post-fertilization using the RNAeasy® Minikit (Qiagen, Hilden, Germany). Embryos were first lysed in 700 µl RTL-Buffer (containing 1% β-mercaptoethanol). The samples were loaded into a QiaSchredder column (Qiagen) and centrifuged at 13,000 rpm for 2 min. 700 µl 70% ethanol was added to the lysate, which was then loaded into the Mini column. After centrifugation, the column was washed with 350 µl RW1 buffer. DNA digestion was performed with the RNAse-free DNase Set (Qiagen). 70 µl RDD buffer was added to 10 µl DNase, loaded into the column, and incubated for 15 min at RT. After DNA digestion, each sample was washed with 300 µl RW1 buffer and twice with 500 µl RPE buffer. The column was centrifuged and dried without adding any buffer. The column was transferred to a new Eppendorf tube, where 30 µl RNase free water was added. The mixture was left to incubate for 1 min and was centrifuged for 2 min at 11,000 rpm. The isolated RNA was either transcribed in cDNA immediately or stored at -80 °C.

Reverse transcription (cDNA synthesis)—In order to transcribe RNA into cDNA, 0.5–1.0 µg RNA was added to 28 µl DEPC water (Applied Biosystems, Foster City, CA).

2.3 μl oligo(dT)15 primers (Promega, Mannheim, Germany) and 2.3 μl random primers (Promega) were added to RNA and incubated for 10 min at 70 °C. The sample was placed on ice and 9.3 μl MMLV buffer (Promega), 2.3 μl dNTPs (Fermentas, Waltham, MA), and 2.3 μl reverse transcriptase (Promega) were added and well mixed. The sample was incubated for 90 min at 42 °C and then 10 min at 70 °C. The cDNA was stored at -20 °C.

Real-time PCR—Real-time PCR (RT-PCR) was carried out using the Light Cycler 480 (Roche Diagnostics, Mannheim, Germany) system. The cDNA was amplified with fast start Taq polymerase, SYBR green (Invitrogen, Darmstadt, Germany), primers for target genes of interest and the following PCR conditions: 5 min at 95 °C, 45 cycles; 10 sec at 95 °C; 10 sec at 60 °C; and 10 sec at 72 °C. Fast start Taq polymerase, buffer, $MgCl_2$ and dNTPs were from the fast start Taq DNA polymerase dNTP pack (Roche Diagnostics). Each PCR test sample was pipetted with Master Mix (1 ml 10x Buffer0.8 ml $MgCl_2$ (25 mM), 0.2 ml dNTPs (10 mM), 0.5 10x SYBR green, 1 ml 0.1% Tween-20, 1.5 ml DEPC water) into 96 well plates, sealed with foil, briefly centrifuged, and measured in Light Cycler 480. The reaction was composed of 10 μl master mix, 1 μl forward primer and 1 μl backward primer, 0.1 μl fast start Taq polymerase, and 6.9 μl DEPC water. The specificity of each primer set was proved by analyzing the melting curve. All the samples were measured in triplicate and normalized with the housekeeping gene hypoxanthin phosphoribosyl transferase 1. The following Primer pairs were used to examine the expression level of dynamin isoforms in zebrafish:

dnm2 fwd: 5′-CTTCAGCTCCATCGGCCAG -3′,

dnm2 rev 5′-TCCTGATCCTCTCGGCAGAA-3′,

dnm1 fwd 5′-AGAACGCAAACCTGGACCTG -3′.

dnm1 rev 5′-AAGCTGCAGGACAAGAGGAC -3′,

dnm1-like fwd 5′-TCAAATTGCAGTGGTGGGGA -3′,

dnm1-like rev 5′-CTGTCCTCTGGGTCTACATGC -3′,

hprt fwd 5′-TCATCATGGACCGAACTGAA -3′,

hprt1 rev 5′-AGCAGCGTCTTCATCGTTTT -3′.

Transmission electron microscopy of zebrafish—Morphant larval zebrafish were sampled at 120 hours post-fertilization and fixed in 1.5% glutaraldehyde/1% PFA and 70 mM Na_3PO_4, pH 7.2. After fixation, the embryos were washed three times in 0.2 M cacodylate buffer and then post-fixed in 1% osmium tetroxide for one hour at room temperature. After rinsing with cacodylate buffer all specimens were dehydrated in a graded ethanol series and infiltrated and embedded with epon according to manufacturer's protocol (Hard Plus Resin 812, Electronmicroscopy Sciences, Hatfield, PA). Thin-sections of 0.5 and 1μm were generated with a Leica RM2165 rotary microtome and stained with 0.5% toluidine blue in a 1% sodium tetraborate solution. When the pronephros was identified on toluidine blue staining, ultra-thin (80—100 nm, thick) sections of the kidney were cut and mounted on slot grids (Luxel, Friday Harbor, WA). The sections were stained with 2% uranyl acetate in distilled water and contrasted with lead citrate. Sections were viewed and

photographed on a JEOL-1230 transmission electron microscope (Eching, Germany) and an attached CCD-camera.

Number of animals per experiment in Figure 1d: wild type, *n* = 144; control, *n* = 128; *dnm2* MO, *n* = 94; *dnm2* MO + *Dnm2*, *n* = 167; *dnm2* MO + Dyn1, *n* = 106; *dnm2* MO + $Dyn1^{E/K}$, *n* = 114; *dnm2* MO + $Dyn1^{K/E}$, *n* = 40; *dnm2* MO + $Dyn1^{I690K}$, *n* = 43; wild type + Bis-T-23, *n* = 57; *dnm2* MO + Bis-T-23, *n* = 57; *dnm2* MO + Dyn1 + Bis-T-23, *n* = 39; *dnm2* MO + $Dyn1^{E/K}$ + Bis-T-23, *n* = 57; *dnm2* MO + $Dyn1^{K/E}$ + Bis-T-23, *n* = 55; *dnm2* MO + $Dyn1^{I690K}$ + Bis-T-23, *n* = 50; Dyn2, *n* = 73; Dyn1, *n* = 94; $Dyn1^{E/K}$, *n* = 74; $Dyn1^{K/E}$, *n* = 95; $Dyn1^{K/E}$ + Bis-T-23, *n* = 40; $Dyn1^{I690K}$, *n* = 119; $Dyn1^{I690K}$ + Bis-T-23, *n* = 44.

Number of animals per experiment in Supplementary Figure 8d: Control MO, *n* = 296; Control MO + DMSO, *n* = 265; *prkce* MO, *n* = 92; *prkce* MO + DMSO, *n* = 78; *prkce* MO + Bis-T-23, *n* = 88; *cd2ap* MO, *n* = 40; *cd2ap* + DMSO, *n* = 91; *cd2ap* + Bis-T-23, *n* = 90; *inf2* MO, *n* = 92; *inf2* MO + DMSO, *n* = 99; *inf2* MO + Bis-T-23, *n*= 74; *nphs1* MO *n* = 114; *nphs1* MO + DMSO, *n* = 64; *nphs1* + Bis-T-23, *n* = 70.

The animal protocol for zebrafish experiments was approved by the Animal Care Committee of the Mount Desert Island Biological Laboratory, Bar Harbor, ME.

Animal studies

Animal strain—BALB/c mice (8 weeks old, males), C57BL/6J (12 weeks old, males), and 129X1/SvJ mice (8 weeks old, males) were from The Jackson Laboratories. Sprague-Dawley rats (8 weeks old, males) were from Charles River Laboratories. $PKC\varepsilon^{KO}$ mice (12 weeks old, mixed genders)[37], $CD2AP^{KO}$ mice (18 days old, mixed genders)[7], ACTN4 mice (12 weeks old, mixed genders)[34] have been described. $DYN1^{R725A}$ (12 weeks old, mixed genders) have been generated in this study (see below).

Pharmacokinetic studies were performed using C57BL/6J male mice by GenScript (Piscataway, NJ). Mice experiments using BALB/c, C57BL/6J, and ACTN4 mice have been approved by the Massachusetts General Hospital Institutional Animal Care and Use Committee, Boston, MA. Mice experiments using $PKC\varepsilon^{KO}$ mice, $CD2AP^{KO}$ mice and Sv/129 mice have been approved by the Lower Saxony State Office for Consumer Protection and Food Safety, Oldenburg, Germany. Mice experiments using $DYN1^{R725A}$ and rats have been approved by the Rush University Medical Center Institutional Animal Care and Use Committee, Chicago, IL.

STZ-induced Type I Diabetic mouse—129X1/SvJ mice (8 weeks old, males) received intraperitoneal injections of Streptozotocin (Sigma-Aldrich, St. Luis, MO) (125 mg/kg body weight) in 50 mmol/l sodium citrate buffer (pH 4.5) or just sodium citrate buffer (vehicle) on day 1 and 4. Blood glucose level was measured every other day with Glucometer Elite (Bayer, Leverkusen, Bayer). Animals with glucose levels > 16mmol/l were regarded as hyperglycemic/diabetic. After 16 weeks of diabetes, the animals were subjected to Bis-T-23 treatment for 8 days.

Urine albumin/creatinine ratio measurements—Spot urine was used to determine levels of albumin and creatinine using either mouse/rat albumin ELISA kit (Bethyl Laboratories, Montgomery, TX) or mouse/rat creatinine ELISA kit (Cayman Chemical, Ann Arbor, MI), respectively, in all animal models except transgenic DYN1^{R725A} mice. Urine samples from Empty (podocine-only transgenic animals) and transgenic DYN1^{R725A} mice were collected by placing them into xurine collection containers for 4 to 6 h. A physical barrier prevented the mixing of solid and liquid wastes, allowing urine samples to be collected free of fecal contamination. Samples were diluted to 1:5, 1:10, or 1:50 with distilled water before total protein was measured using a mouse albumin ELISA kit (Bethyl Laboratories, Montgomery, TX) and urine creatinine measurements were taken using an ELISA kit (Cayman Chemical, Ann Arbor, MI). Absorbances were measured using EnSpire 2300 Multilabel Reader (Perkin Elmer, Waltham, MA). No data points have been excluded. Data were plotted as mean ± SD and statistical significance was determined using unpaired *t*-test calculated using Prism software (GraphPad, La Jolla, CA).

BU (blood urea) measurements—BU measurements were performed on the mice serum collected from the eye vein using QuantiCrom™ Urea Assay Kid (BioAssay Systems, Hayward, CA) based on the manufacturer's protocol.

LPS and PAN induced proteinuria in rodents—BALB/c mice (8 weeks old, males) were injected intraperitoneally with LPS (200 μg/mouse) twice with a 24 h interval. When indicated in the figure, 24 h after the second injection, mice received single intraperitoneal injection of Bis-T-23 (40 mg/kg) or DMSO (20%). PAN (150 mg/kg body weight) was injected into a tail vein of Sprague-Dawley rats (male 8 weeks old) and urine albumin/creatinine ration was measured as described above.

Glomerular filtration rate (GFR) and renal plasma flow (RPF) (Inulin- and PAH-clearance)—Measurements of RPF by PAH clearance and of GFR by inulin clearance were performed 8 days after daily treatment of C57Bl/6N male mice (weighing 22–25 g) (n = 6 in each group). The mice were anesthetized using isoflurane in order to measure only the RPF and GFR of the post-ischemic kidney. For urine collection, a catheter was placed into the bladder and the tail vein was canulated to infuse inulin and para-aminohippuric acid (PAH). After a one-hour equilibration period, urine was collected for 90min and blood was drawn at the end of the infusion. The infusion was performed with 15% inulin, 3.75% PAH, and 1% bovine albumin in 0.9% saline at a rate of 5 μl/min. Inulin concentrations in both urine and plasma aliquots were measured using the standard colorimetric methods. For invasive blood pressure measurements, RR was determined eight days after daily treatment with Bis-T-23 or DMSO (n=3 per group). Hemodynamic measurements were assessed by Millar catheter in anesthetized mice as described previously[57]. In brief, after the mice were anesthetized, a catheter was placed in the carotid artery and RR-measurements were captured constantly over eight minutes.

Generation of DYN1^{R725A} transgenic mice

The construct to generate DYN1^{R725A} transgenic mice was made using the BD Creator™ Cloning System (BD Biosciences, San Jose, CA; Clontech, Mountain View, CA). Briefly, a

2.5 kb fragment containing the full-length cDNA of human *DNM1* with a mutation in R725A was isolated from pcDNA-*DNM1*^{R725A} through restriction digest with *Hind*III and *Bam*HI. The 2.5 kb fragment was isolated, blunt-ended, and cloned into the *Sma*I site of pDNR-1r (donor vector). The proper orientation of the cDNA was confirmed by restriction enzyme digest mapping. The *DNM1*^{R725A} cDNA was then transferred from the donor vector to pLP-Tre2, an inducible tet-responsive expression vector, using Cre-loxP site-specific recombination. The 6.1 kb inducible tetO-*DNM1*^{R725A} construct was released from the vector backbone by *Ase*I digest, purified by gel-extraction (QIAquick Gel Extraction Kit, Qiagen), and used for injections into the pronuclei of fertilized oocytes of FvB/NJ mice. Transgenic founder mice were identified by PCR using the same set of primers used to genotype the first and subsequent offspring.

DNM1-TG-Forward: CTTCTTGCCTCGAGGATCTG

DNM1-TG-Reverse: AATTGGCCAGGTCAGAGTTG

Transgenic founders were mated to FvB/NJ mice to expand the colony and to Podocin-rt-TA mice[58] in FvB/NJ background to generate double transgenic doxycycline-inducible Podocin-rt-TA/tetO-*DNM1*^{R725A} (*DNM1*$^{R725A/R725A}$) mice. Double transgenic mice were identified using the above-mentioned primers and primers specific for the human Podocin promoter of the Podocin-rt-TA mice:

Nphs2-Forward: CCTGCTCCATTCTTGGAATG;

Nphs2-Reverse: GCTTATGCCTGATGTTGATGATGC

PCR conditions were: 94°C, 2 min, 1 cycle; 94°C, 20 sec, 57°C, 40 sec, 72°C, 1 min for 30 cycles followed by a final extension step of 7 min at 72°C.

Finally, Podocin-rt-TA/tetO-*DNM1*^{R725A} F1 littermates were mated to obtain F2 double transgenic mice (DYN1^{R725A}) for experimental procedures. To induce expression of Dyn1^{R725A} *in vivo*, mice were fed with chow containing 2000 ppm doxycycline chow for at least one week.

Histological analysis

For histological analysis, the mice were anesthetized with isoflurane and perfused first with saline and then fixation solution (0.15% 1M HEPES buffer, 1.5% glutaraldehyde, 1.5% paraformaldehyde, pH 7.35) via the left ventricle. The kidneys were harvested and 1 × 1 mm cubes were cut from the cortex part of the kidney and fixed overnight in fixation solution. The tissue cubes were post-fixed with osmium in cacodylate buffer and contrasted with 4% uranyl acetate at 4°C. Finally, the samples were dehydrated in acetone and embedded in EPON/acetone (1:1).

PAS (Periodic Acid-Schiff) staining—PAS staining was performed on paraffin-embedded tissue sections following a standard protocol. In brief, the kidney tissue sections were first deparaffinised via the following steps: 3x 5 min Histoclear (Life Science Products, Frederick, CO), 3x 3 min 100% ethanol, 2x 2 min 96% ethanol, 1x 1 min 70% ethanol, briefly in distilled water. The deparaffinised sections were oxidized in 0.5% periodic acid for 10 min, washed 3x 5 min with distilled water, and incubated in Schiff's reagent for 20

min. The differentiation was carried out in sulfite water (12 ml 10% Na_2SO_3, 10 ml 1M HCl, 200 ml distilled water) 3x for 2 min and a 10 min wash under running tap water. The sections were dehydrated in following steps: 2x briefly 96%, 3x 2 min 100% ethanol, 3x 2 min Histoclear, and covered with Histokitt. The PAS staining was documented using a Leica DMLB microscope with a Leica DFC425C camera (Leica, Wetzlar, Germany).

Collagen IV staining—Paraffin-embedded kidney tissue sections were deparaffinised as described in PAS staining and pretreated by incubation with 1mg/ml trypsin (Sigma-Aldrich, St. Luis, MO) at 37°C for 30 min. To block, the sections were then incubated with 10% donkey serum (Jackson Immuno Research, Suffolk, England) and diluted in TBS (50 mM Tris-HCl, 150 mM NaCl, pH 7.6) for 30 min at RT. The sections were incubated with 1:50 diluted Collagen IV antibody (Southern Biotech, Birmingham, AL) at 4°C overnight. On the second day the unbound primary antibodies were washed away by rinsing 3x 5 min with TBS and the sections were incubated with anti-goat Alexa Fluor 555 (Invitrogen, Carlsbad, CA) for 1 h at room temperature. The sections were again washed 3x 5 min with TBS and mounted with Aquapolymount medium (Polysciences Inc., Warrington, PA). The staining was analyzed under Leica DMLB microscopy with a Leica DFC425C camera.

Toluidine blue staining—One micron thick sections were cut using glass knives and a Sorvall MT-1 (Dupont, Wilmington, DE) ultramicrotome and floated on water droplets on glass slides. The slides were dried in a humidity chamber on a warm hot plate. Toluidine blue stain (0.5% toluidine blue in aqueous 0.5% sodium borate) was pipetted over the sections and placed onto the hot plate until a slight gold rim could be seen around the stain droplet. The sections were rinsed in a stream of distilled water, dried, placed on cover slips, and examined by light microscopy. Representative sections were chosen and the blocks were trimmed accordingly. Thin sections were cut using a diamond knife and an LKB 2088 ultramicrotome (LKB, Stockholm, Sweden) and then placed on copper grids. Sections were stained with lead citrate and examined in a FEI Morgagni transmission electron microscope (FEI, Hillsboro, OR). Images were captured with an AMT (Advanced Microscopy Techniques, Woburn, MA) 2K digital CCD camera.

Transmission and scanning electron microscopy

For scanning electron microscopy, renal tissues were dissected and sliced thinly into 2 mm pieces. The tissues were fixed in 4% PFA overnight, washed 3x in PBS, dehydrated, critically point dried using the 850 Critical Point Dryer (EMS) and sputter coated in gold on the 108 Auto Sputter Coater (Cressington, Watford, England). For TEM, renal tissues were collected and dissected into 2–3 mm pieces. The tissues were fixed in 4% PFA O/N, washed 3x in 0.1M cacodylate buffer and post fixed in 1% OsO4 for 1 hours. Tissues were once again washed, dehydrated and embedded in Epon812. Ultrathin kidney sections (70 nm) obtained on the EM UC7 Ultramicrotome (Leica) were mounted onto Formvar coated Ni slot grids (EMS). Grids were stained for 15 min in 5% uranyl acetate followed by 0.1% lead citrate for 5 min. SEM and TEM were done on the same scope (Sigma HDVP Electron Microscope). Electron microscopy micrographs were obtained using the Sigma HDVP Electron Microscope (Zeiss).

Foot process longitudinal length measurements—Scanning electron microscopy images were used to measure longitudinal length from the beginning of each final branch point to the end of a foot process. Each measurement was analyzed using Image J. 'Foot process length' from each animal was averaged from a total of 100 measured processes. Briefly, 15–18 individual foot processes were traced from each image taken from 5–6 different glomeruli of each genotype by a naïve observer. Data were plotted as mean ± SD and statistical significance was determined using unpaired *t*-test calculated using Prism software (GraphPad, La Jolla, CA).

Statistical analysis

Statistical analysis was performed using GraphPad Prism software (GraphPad Software, Inc.). Results are depicted as median ± SD. For a two-group comparison, a Student's *t*-test was applied if the pretest for normality (D'Agostino-Pearson normality test) was not rejected at the 0.05 significance level. *P* values less than 0.05 were considered significant. No statistical method was used to predetermine sample size. Survival was determined using log-rank (Mantel-Cox) test from GraphPad Prism software package. Survival *P* value tested the null hypothesis that the survival curves are identical in the two populations and is not rejected if *P* value equals 1.0 minus half the two-tail *P* value. *P* value less then 0.05 is considered statistically significant.

Supplementary Material

Refer to Web version on PubMed Central for supplementary material.

Acknowledgments

This work was supported by the National Institutes of Health (R01 DK093773 and DK087985 to S.S.), the NephCure Foundation (S.S.), and Deutsche Forschungsgemeinschaft (SCHI587/3, 4, 6 to M.S. and REBIRTH 2 to D.H.–K. and S.E.). N.H. is the recipient of the New Investigator Award from Mount Desert Island Biological Laboratory. The DNA encoding genes for PKCε and mutant with impaired kinase activity were gift from J-W. Soh, Inha University, Incheon, South Korea. Immortalized podocytes from ACTN4 mice, ACTN4 mice and morpholino to downregulate *inf-2* were gift from M. Pollak, Beth Israel Deaconess Medical Center, Boston, MA. Tg (L-FABP:DBP-EGFP) and Tg (l-fabp:DBP-EGFP) zebrafish were gift from J. Xie and B. Anand-Apte, Cleveland Clinic, Cleveland, OH. PKCε^{KO} mice were gift from M. Leitges, University of Oslo, Oslo, Norway. CD2AP^{KO} mice were gift from A. Shaw, Washington University, St. Louis, MO.

References

1. Meguid El Nahas A, Bello AK. Chronic kidney disease: the global challenge. Lancet. 2005; 365:331–340. [PubMed: 15664230]
2. Saran R, Hedgeman E, Huseini M, Stack A, Shahinian V. Surveillance of chronic kidney disease around the world: tracking and reining in a global problem. Adv Chronic Kidney Dis. 2010; 17:271–281. [PubMed: 20439096]
3. Haraldsson B, Nystrom J, Deen WM. Properties of the glomerular barrier and mechanisms of proteinuria. Physiol Rev. 2008; 88:451–487. [PubMed: 18391170]
4. Brown EJ, et al. Mutations in the formin gene INF2 cause focal segmental glomerulosclerosis. Nat Genet. 2010; 42:72–76. [PubMed: 20023659]
5. Boyer O, et al. Mutations in INF2 are a major cause of autosomal dominant focal segmental glomerulosclerosis. J Am Soc Nephrol. 2011; 22:239–245. [PubMed: 21258034]
6. Santin S, et al. Nephrin mutations cause childhood- and adult-onset focal segmental glomerulosclerosis. Kidney Int. 2009; 76:1268–1276. [PubMed: 19812541]

7. Shih NY, et al. Congenital nephrotic syndrome in mice lacking CD2-associated protein. Science. 1999; 286:312–315. [PubMed: 10514378]
8. Kaplan JM, et al. Mutations in ACTN4, encoding alpha-actinin-4, cause familial focal segmental glomerulosclerosis. Nat Genet. 2000; 24:251–256. [PubMed: 10700177]
9. Pagtalunan ME, et al. Podocyte loss and progressive glomerular injury in type II diabetes. The Journal of clinical investigation. 1997; 99:342–348. [PubMed: 9006003]
10. Faul C, Asanuma K, Yanagida-Asanuma E, Kim K, Mundel P. Actin up: regulation of podocyte structure and function by components of the actin cytoskeleton. Trends Cell Biol. 2007; 17:428–437. [PubMed: 17804239]
11. Wiggins RC. The spectrum of podocytopathies: a unifying view of glomerular diseases. Kidney Int. 2007; 71:1205–1214. [PubMed: 17410103]
12. Jefferson JA, Alpers CE, Shankland SJ. Podocyte biology for the bedside. Am J Kidney Dis. 2011; 58:835–845. [PubMed: 21715071]
13. Tryggvason K, Patrakka J, Wartiovaara J. Hereditary proteinuria syndromes and mechanisms of proteinuria. The New England journal of medicine. 2006; 354:1387–1401. [PubMed: 16571882]
14. Ronco P. Proteinuria: is it all in the foot? The Journal of clinical investigation. 2007; 117:2079–2082. [PubMed: 17671644]
15. Seiler MW, Rennke HG, Venkatachalam MA, Cotran RS. Pathogenesis of polycation-induced alterations (“fusion”) of glomerular epithelium. Lab Invest. 1977; 36:48–61. [PubMed: 63647]
16. Reiser J, Sever S. Podocyte biology and pathogenesis of kidney disease. Annu Rev Med. 2013; 64:357–366. [PubMed: 23190150]
17. Sever S, et al. Proteolytic processing of dynamin by cytoplasmic cathepsin L is a mechanism for proteinuric kidney disease. The Journal of clinical investigation. 2007; 117:2095–2104. [PubMed: 17671649]
18. Soda K, et al. Role of dynamin, synaptojanin, and endophilin in podocyte foot processes. The Journal of clinical investigation. 2012; 122:4401–4411. [PubMed: 23187129]
19. Mettlen M, Pucadyil T, Ramachandran R, Schmid SL. Dissecting dynamin’s role in clathrin-mediated endocytosis. Biochemical Society transactions. 2009; 37:1022–1026. [PubMed: 19754444]
20. Sever S, Chang J, Gu C. Dynamin rings: not just for fission. Traffic. 2013; 14:1194–1199. [PubMed: 23980695]
21. Hinshaw JE. Dynamin and its role in membrane fission. Annual review of cell and developmental biology. 2000; 16:483–519.
22. Gu C, et al. Direct dynamin-actin interactions regulate the actin cytoskeleton. The EMBO journal. 2010; 29:3593–3606. [PubMed: 20935625]
23. Ross JA, et al. Dimeric endophilin A2 stimulates assembly and GTPase activity of dynamin 2. Biophysical journal. 2011; 100:729–737. [PubMed: 21281588]
24. Hill T, et al. Small molecule inhibitors of dynamin I GTPase activity: development of dimeric tyrphostins. Journal of medicinal chemistry. 2005; 48:7781–7788. [PubMed: 16302817]
25. Gu C, et al. Regulation of Dynamin Oligomerization in Cells: The Role of Dynamin-Actin Interactions and Its GTPase Activity. Traffic. 2014; 15:819–838. [PubMed: 24891099]
26. Gibbs EM, et al. Two dynamin-2 genes are required for normal zebrafish development. PLoS One. 2013; 8:e55888. [PubMed: 23418470]
27. Hanke N, et al. “Zebrafishing” for novel genes relevant to the glomerular filtration barrier. BioMed research international. 2013; 2013:658270. [PubMed: 24106712]
28. Hentschel DM, et al. Rapid screening of glomerular slit diaphragm integrity in larval zebrafish. Am J Physiol Renal Physiol. 2007; 293:F1746–1750. [PubMed: 17699558]
29. Kirsch T, et al. Knockdown of the hypertension-associated gene NOSTRIN alters glomerular barrier function in zebrafish (Danio rerio). Hypertension. 2013; 62:726–730. [PubMed: 23959558]
30. Song BD, Yarar D, Schmid SL. An assembly-incompetent mutant establishes a requirement for dynamin self-assembly in clathrin-mediated endocytosis in vivo. Molecular biology of the cell. 2004; 15:2243–2252. [PubMed: 15004222]

31. Faul C, et al. The actin cytoskeleton of kidney podocytes is a direct target of the antiproteinuric effect of cyclosporine A. Nature medicine. 2008; 14:931–938.
32. Pippin JW, et al. Inducible rodent models of acquired podocyte diseases. American journal of physiology Renal physiology. 2009; 296:F213–229. [PubMed: 18784259]
33. Sever S, Muhlberg AB, Schmid SL. Impairment of dynamin's GAP domain stimulates receptor-mediated endocytosis. Nature. 1999; 398:481–486. [PubMed: 10206643]
34. Henderson JM, Al-Waheeb S, Weins A, Dandapani SV, Pollak MR. Mice with altered alpha-actinin-4 expression have distinct morphologic patterns of glomerular disease. Kidney Int. 2008; 73:741–750. [PubMed: 18185509]
35. Yao J, et al. Alpha-actinin-4-mediated FSGS: an inherited kidney disease caused by an aggregated and rapidly degraded cytoskeletal protein. PLoS Biol. 2004; 2:e167. [PubMed: 15208719]
36. Tossidou I, et al. CIN85/RukL is a novel binding partner of nephrin and podocin and mediates slit diaphragm turnover in podocytes. The Journal of biological chemistry. 2010; 285:25285–25295. [PubMed: 20457601]
37. Meier M, et al. Deletion of protein kinase C-epsilon signaling pathway induces glomerulosclerosis and tubulointerstitial fibrosis in vivo. J Am Soc Nephrol. 2007; 18:1190–1198. [PubMed: 17360953]
38. Akita Y. Protein kinase Cepsilon: novel aspects of its multiple functions in cellular signaling. FEBS J. 2008; 275:3987. [PubMed: 18637122]
39. Chhabra ES, Higgs HN. INF2 Is a WASP homology 2 motif-containing formin that severs actin filaments and accelerates both polymerization and depolymerization. The Journal of biological chemistry. 2006; 281:26754–26767. [PubMed: 16818491]
40. Ruotsalainen V, et al. Nephrin is specifically located at the slit diaphragm of glomerular podocytes. Proc Natl Acad Sci U S A. 1999; 96:7962–7967. [PubMed: 10393930]
41. Graham ML, Janecek JL, Kittredge JA, Hering BJ, Schuurman HJ. The streptozotocin-induced diabetic nude mouse model: differences between animals from different sources. Comp Med. 2011; 61:356–360. [PubMed: 22330251]
42. Giganti A, Friederich E. The actin cytoskeleton as a therapeutic target: state of the art and future directions. Prog Cell Cycle Res. 2003; 5:511–525. [PubMed: 14593746]
43. Schiff PB, Fant J, Horwitz SB. Promotion of microtubule assembly in vitro by taxol. Nature. 1979; 277:665–667. [PubMed: 423966]
44. Altschuler Y, et al. Redundant and distinct functions for dynamin-1 and dynamin-2 isoforms. The Journal of cell biology. 1998; 143:1871–1881. [PubMed: 9864361]
45. Gowrishankar K, et al. Active remodeling of cortical actin regulates spatiotemporal organization of cell surface molecules. Cell. 2012; 149:1353–1367. [PubMed: 22682254]
46. Byron A, et al. Glomerular cell cross-talk influences composition and assembly of extracellular matrix. J Am Soc Nephrol. 2014; 25:953–966. [PubMed: 24436469]
47. Menon MC, Chuang PY, He CJ. The glomerular filtration barrier: components and crosstalk. Int J Nephrol. 2012; 2012:749010. [PubMed: 22934182]
48. Shankland SJ, Pippin JW, Duffield JS. Progenitor cells and podocyte regeneration. Semin Nephrol. 2014; 34:418–428. [PubMed: 25217270]
49. Daehn I, et al. Endothelial mitochondrial oxidative stress determines podocyte depletion in segmental glomerulosclerosis. The Journal of clinical investigation. 2014; 124:1608–1621. [PubMed: 24590287]
50. Quan A, Robinson PJ. Rapid purification of native dynamin I and colorimetric GTPase assay. Methods in enzymology. 2005; 404:556–569. [PubMed: 16413300]
51. Leonard M, Song BD, Ramachandran R, Schmid SL. Robust colorimetric assays for dynamin's basal and stimulated GTPase activities. Methods in enzymology. 2005; 404:490–503. [PubMed: 16413294]
52. Mundel P, Reiser J, Kriz W. Induction of differentiation in cultured rat and human podocytes. Journal of the American Society of Nephrology: JASN. 1997; 8:697–705. [PubMed: 9176839]

53. Worthmann K, et al. Def-6, a novel regulator of small GTPases in podocytes, acts downstream of atypical protein kinase C (aPKC) lambda/iota. Am J Pathol. 2013; 183:1945–1959. [PubMed: 24096077]
54. Yao J, et al. Alpha-actinin-4-mediated FSGS: an inherited kidney disease caused by an aggregated and rapidly degraded cytoskeletal protein. PLoS Biol. 2004; 2:e167. [PubMed: 15208719]
55. Schiffer M, Mundel P, Shaw AS, Bottinger EP. A novel role for the adaptor molecule CD2-associated protein in transforming growth factor-beta-induced apoptosis. The Journal of biological chemistry. 2004; 279:37004–37012. [PubMed: 15213232]
56. Sever S, et al. Proteolytic processing of dynamin by cytoplasmic cathepsin L is a mechanism for proteinuric kidney disease. The Journal of clinical investigation. 2007; 117:2095–2104. [PubMed: 17671649]
57. Xie J, Farage E, Sugimoto M, Anand-Apte B. A novel transgenic zebrafish model for blood-brain and blood-retinal barrier development. BMC developmental biology. 2010; 10:76. [PubMed: 20653957]
58. Hentschel DM, et al. Rapid screening of glomerular slit diaphragm integrity in larval zebrafish. Am J Physiol Renal Physiol. 2007; 293:F1746–1750. [PubMed: 17699558]
59. Hanke N, et al. “Zebrafishing” for novel genes relevant to the glomerular filtration barrier. BioMed research international. 2013; 2013:658270. [PubMed: 24106712]
60. Ashworth S, et al. Cofilin-1 inactivation leads to proteinuria--studies in zebrafish, mice and humans. PLoS One. 2010; 5:e12626. [PubMed: 20838616]
61. Meier M, et al. Deletion of protein kinase C-epsilon signaling pathway induces glomerulosclerosis and tubulointerstitial fibrosis in vivo. J Am Soc Nephrol. 2007; 18:1190–1198. [PubMed: 17360953]
62. Shih NY, et al. Congenital nephrotic syndrome in mice lacking CD2-associated protein. Science. 1999; 286:312–315. [PubMed: 10514378]
63. Henderson JM, Al-Waheeb S, Weins A, Dandapani SV, Pollak MR. Mice with altered alpha-actinin-4 expression have distinct morphologic patterns of glomerular disease. Kidney Int. 2008; 73:741–750. [PubMed: 18185509]
64. Hilfiker-Kleiner D, et al. A cathepsin D-cleaved 16 kDa form of prolactin mediates postpartum cardiomyopathy. Cell. 2007; 128:589–600. [PubMed: 17289576]
65. Shigehara T, et al. Inducible podocyte-specific gene expression in transgenic mice. J Am Soc Nephrol. 2003; 14:1998–2003. [PubMed: 12874453]

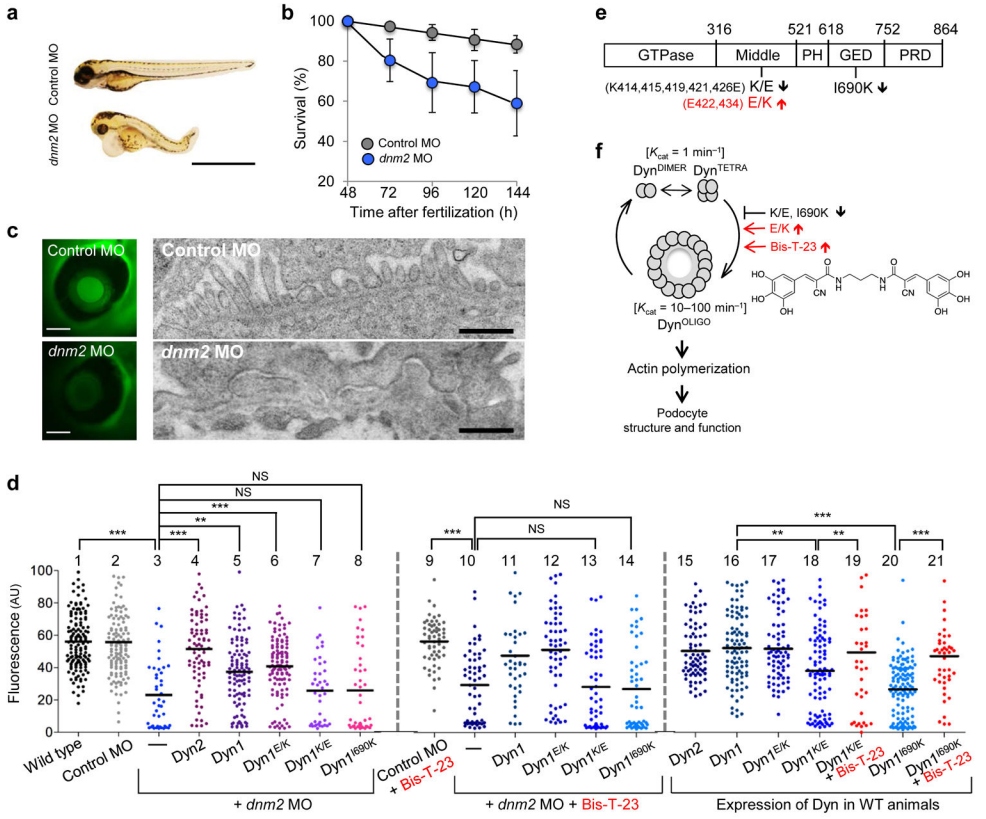

Figure 1.

Dynamin oligomerization is essential for kidney function. (**a**) Phenotype of zebrafish larvae injected with either scrambled (Control MO) or dynamin-2-specific morpholino (*dnm2* MO) 120 hours post-fertilization. Scale bars, 2 mm. (**b**) Survivorship curves of zebrafish larvae injected with either Control MO or *dnm2* MO. Each curve represents 180 animals for Control MO and 245 animals for *dnm2* MO. Error bars, mean ± SD (log-rank: $P < 0.0001$ for comparison of mean survival time). (**c**) Representative image of the fluorescence of circulating eGFP-DBP in the retinal vessel plexus of the fish eye 96 hours post-fertilization and injected with either control MO or *dnm2* MO (left) ($n = 128$ images for control MO, and $n = 94$ images for *dnm2* MO animals). Scale bars, 100 μm. Transmission electron micrographs of glomeruli analyzed in zebrafish larvae 120 hours post-fertilization and injected with either control MO or *dnm2* MO (right). Scale bars, 0.5 μm. (**d**) Intensity of circulating eGFP-DBP (AU, arbitrary units) in the retinal vessel plexus of the fish eye 96 hours post-fertilization and treated with the indicated MO and/or expression construct and with Bis-T-23 (1 ng per larvae) or with DMSO as vehicle (20% per larvae). For groups 1–6, 16, and 20, $n = 100–150$; for all other groups $n = 40–100$. Black lines represent median intensity in each group (**$P \leq 0.01$, ***$P \leq 0.001$, unpaired *t*-test). (**e**) A schematic diagram indicating the domain structures of dynamin: GTPase, Middle, PH (Pleckstrin-Homology), GED (GTPase Effector Domain), and PRD (Proline/arginine-Rich Domain). Indicated mutations: K/E (K-to-E mutations of the indicated amino acid residues in black), E/K (E-to-K mutations of the indicated residues in red) and I690K. (**f**) A schematic diagram indicating that dimers of dynamin (Dyn^{DIMER}) and tetramers of dynamin (Dyn^{TETRA}) exhibit basal

rate of GTP hydrolysis. Oligomerized dynamin (Dyn^{OLIGO}), whose formation is promoted by Bis-T-23 (structure shown at right) or through indicated mutations, exhibits increased rate of GTP hydrolysis. Dyn^{OLIGO} induces actin polymerization and crosslinking of F-actin, which in turn regulates the structure and function of podocytes. The small arrows in **e** and **f** indicate the effect of the mutations on dynamin's propensity to oligomerize.

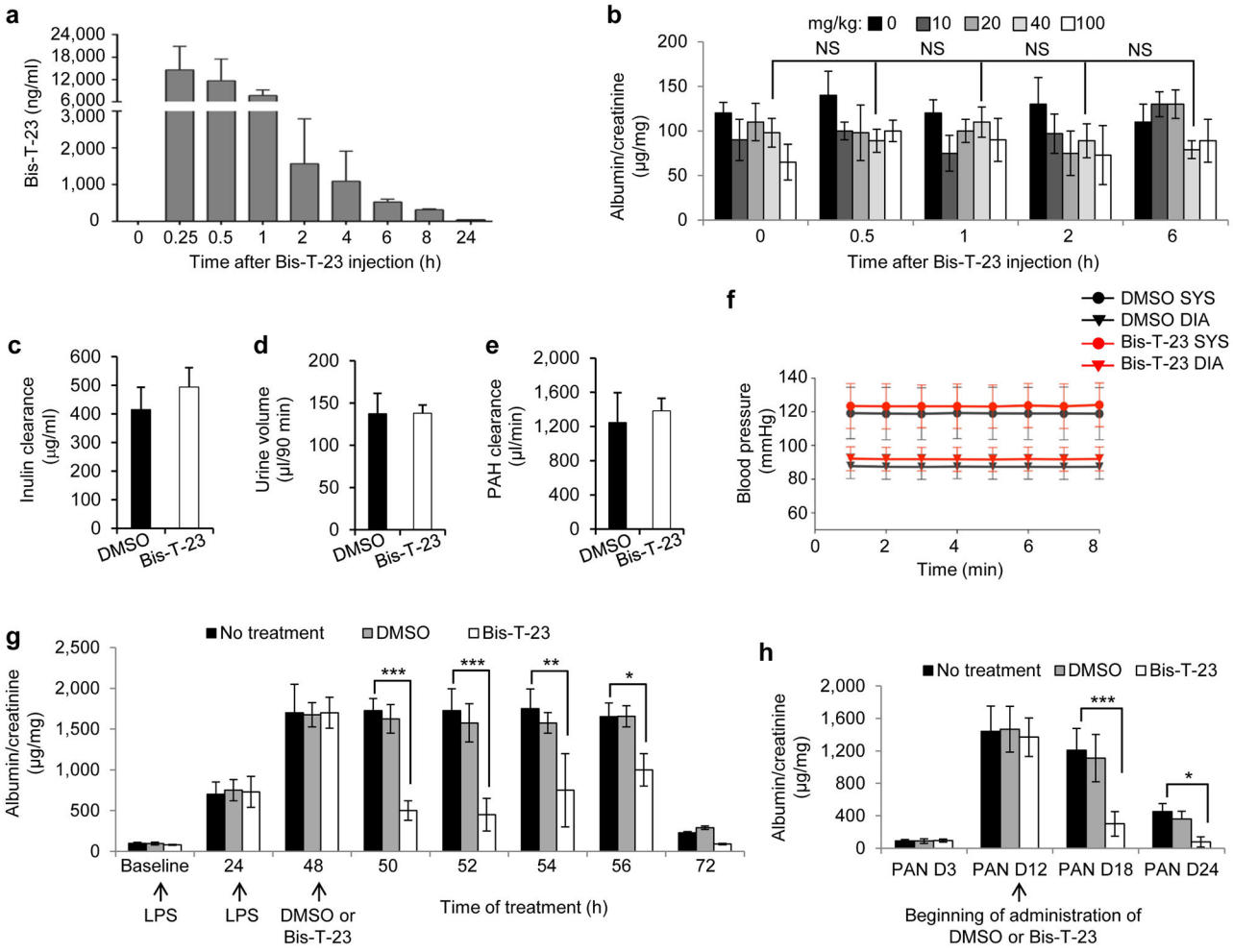

Figure 2.

Dynamin oligomerization ameliorates transient proteinuria. (**a**) Plasma pharmacokinetics of Bis-T-23 after injection (40 mg/kg) in C57BL/6J mice (n = 3) as measured by mass spectrometry. (**b**) Proteinuria of C57BL/6J mice determined by spot urine test before injection (0 h) and at the indicated hours after injection of the indicated concentrations of Bis-T-23. NS, not statistically significant (unpaired t-test; n = 5 mice per concentration). (**c**-**e**) Inulin clearance (**c**), urine volume (**d**) and para-aminohippurate (PAH) clearance (**e**) of C57BL/6J mice determined after 8 consecutive days of treatment with DMSO (1%, vehicle) or Bis-T-23 (40 mg/kg). Error bars, mean ± SD (n = 6 mice per condition). (**f**) The systolic (SYS) or diastolic (DIA) blood pressure of 129X1/SvJ mice measured invasively using a carotid catheter after 8 consecutive days of treatment with DMSO (1%, vehicle) or Bis-T-23 (40 mg/kg) (n = 3 mice per condition). (**g**) Proteinuria of BALB/c mice determined by spot urine test at indicated times after two consecutive doses of LPS. As indicated, animals were injected with either DMSO (1%, vehicle) or Bis-T-23 (40 mg/kg) (n = 10 mice per condition). Error bars, mean ± SD (*$P \leq 0.05$; **$P \leq 0.01$, ***$P \leq 0.001$, unpaired t-test). (**h**) Proteinuria of Sprague-Dawley rats treated with PAN and determined by spot urine test. Rats were treated once a day starting 12 days after PAN with DMSO (1%, vehicle) or Bis-

T-23 (20 mg/kg) for 6 consecutive days (n = 6 rats per condition). Error bars, mean ± SD (*$P \leq 0.05$; ***$P \leq 0.001$, unpaired t-test).

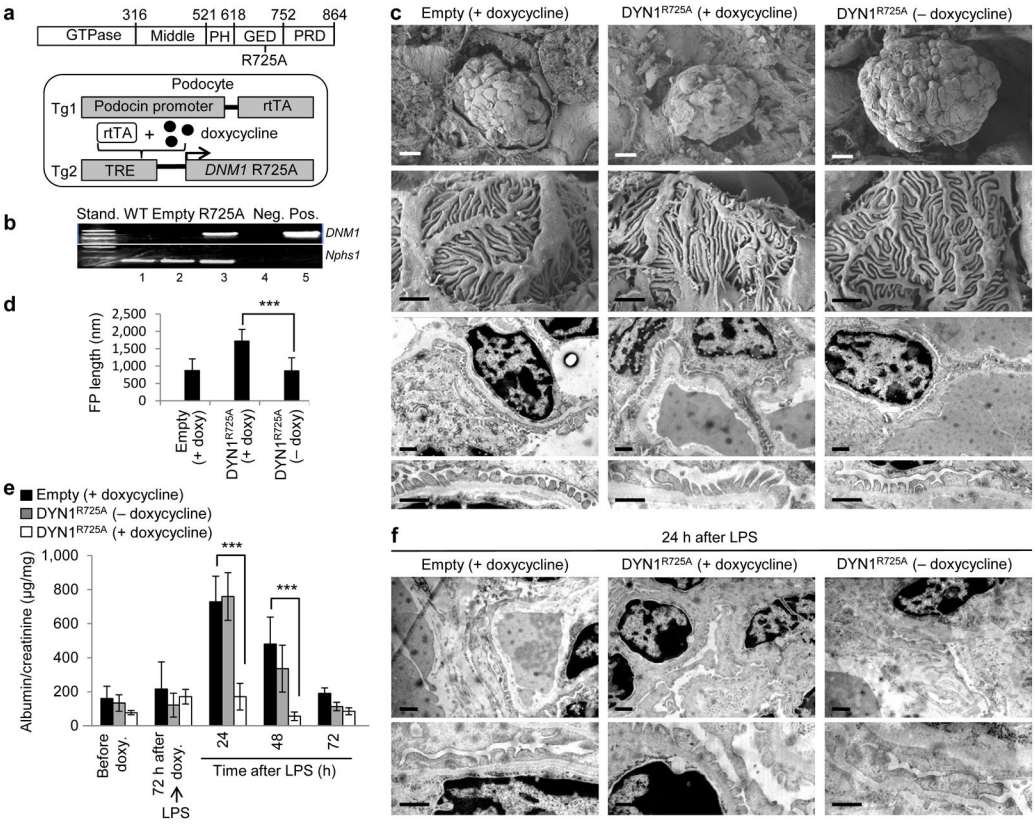

Figure 3.

Dynamin oligomerization in podocytes protects against proteinuria. (**a**) Domain structure of dynamin (top). R725A mutation is situated in the GED, which renders dynamin prone to oligomerize. A schematic diagram (bottom) indicating that the human gene *DNM1* carrying R725A mutation (*DNM1*^{R725A}) was placed under the regulation of a tetracycline-responsive promoter element (TRE; tetO). This transgenic mouse (Tg2) was subsequently bred to a second transgenic strain expressing the reverse tetracycline-transactivator (tTA) protein under the control of a podocin-specific promoter to allow for podocyte-specific gene expression (Tg1). Expression of *DNM1*^{R725A} was induced by administration of the tetracycline analog, doxycycline. (**b**) RT-PCR of *DNM1* from wild-type mice (WT), podocin-Cre only transgenic mice (Empty) fed with doxycycline and homozygous *DNM1*$^{R725A/R725A}$ transgenic mice (R725A) fed with doxycycline. Neg, negative control with water as a template; Pos, positive control with plasmid encoding *DNM1*^{R725A}. Nephrin (*Nphs1*) was used as a positive control. (**c**) Representative electron micrographs of glomeruli (n = 5–6 glomeruli per genotype) from Empty and R725A transgenic mice fed with either a normal diet (− doxycycline) or doxycycline diet (+ doxycycline). Rows 1 (scale bars, 10 µm), and 2 (scale bars, 1 µm) show scanning electron microscopy. Rows 3 and 4 (scale bars, 1 µm) show transmission electron microscopy (TEM) images. (**d**) Length of foot processes determined by analyzing images in **d**. Doxycycline (doxy) (**e**) Proteinuria determined by analysis of spot urine samples at indicated times and in the indicated genotypes. Mice were fed with doxycycline (doxy) diet before they were injected with LPS (n = 6 mice per condition). Error bars, mean ± SD (***$P \leq 0.001$, unpaired t-test). (**f**) Representative TEM

images of glomeruli (n = 5–6 glomeruli per genotype) from Empty and R725A transgenic mice 24 hours after LPS injection. Animals were fed with either a normal diet (− doxycycline) or doxycycline diet (+ doxycycline). Scale bars, 2 μm (top row) and 1 μm (bottom row).

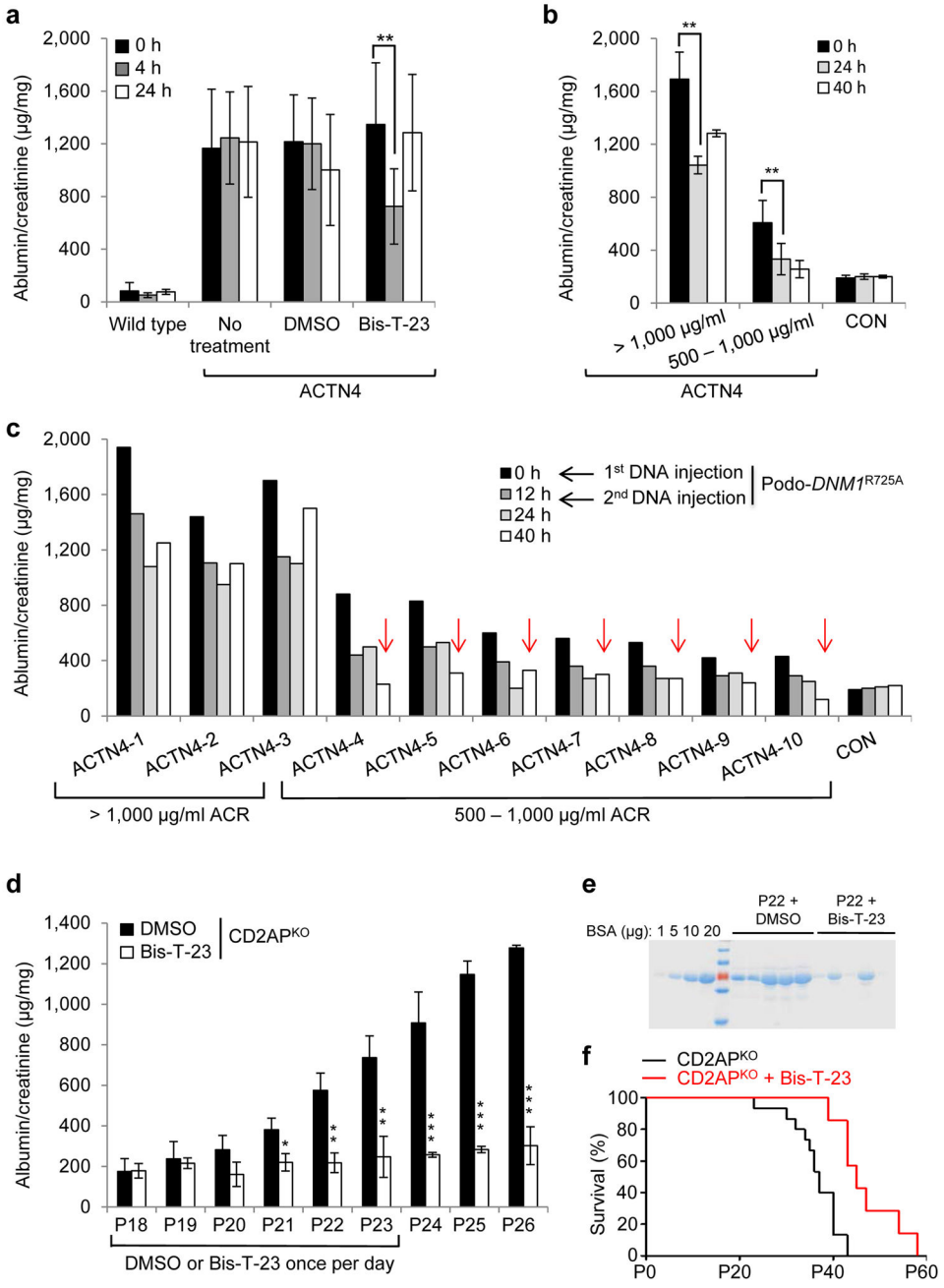

Figure 4.

Dynamin oligomerization targets actin cytoskeleton in podocytes. (**a**) Proteinuria in wild type and ACTN4 mice (without treatment or with treatment with either DMSO (1%, vehicle) or with Bis-T-23 (40 mg/kg)) as determined by spot urine test at indicated time points. Error bars, mean ± SD (**$P \leq 0.01$, unpaired *t*-test). (**b**,**c**) Proteinuria in ACTN4 mice determined by spot urine test prior to and after double injection of a podocin-driven expression vector encoding DNM1^{R725A} mutant protein. Animals were grouped by protein levels before treatment ($n = 3$ for > 1,000 µg/ml ACR; $n = 7$ for 500–1,000 µg/ml ACR). Individual animals from **b** are shown in **c**. Red arrows indicate reduction of proteinuria to

control levels. Error bars, mean ± SD (**$P \leq 0.01$, unpaired *t*-test). (**d**) Proteinuria in CD2AP^{KO} mice determined by spot urine test over several days during which animals were treated daily with DMSO (1%, vehicle) or Bis-T-23 (40 mg/kg), starting at Postnatal Day 18 ($n = 5$ mice per condition). Error bars, mean ± SD (*$P \leq 0.05$; **$P \leq 0.01$, ***$P \leq 0.001$, unpaired *t*-test). (**e**) Coomassie blue staining of SDS-PAGE gel showing protein bands from two microliters of mouse spot urine at day 22 in **d**. BSA was used as a standard. (**f**) Line graph depicting number of live CD2AP^{KO} mice (black lines, $n = 20$ mice) and CD2AP^{KO} mice injected daily with Bis-T-23 (40 mg/kg) (red lines, $n = 7$ mice) at indicated time points. Animals exhibited a statistically significant difference in survival rate (log-rank: $P < 0.0163$).

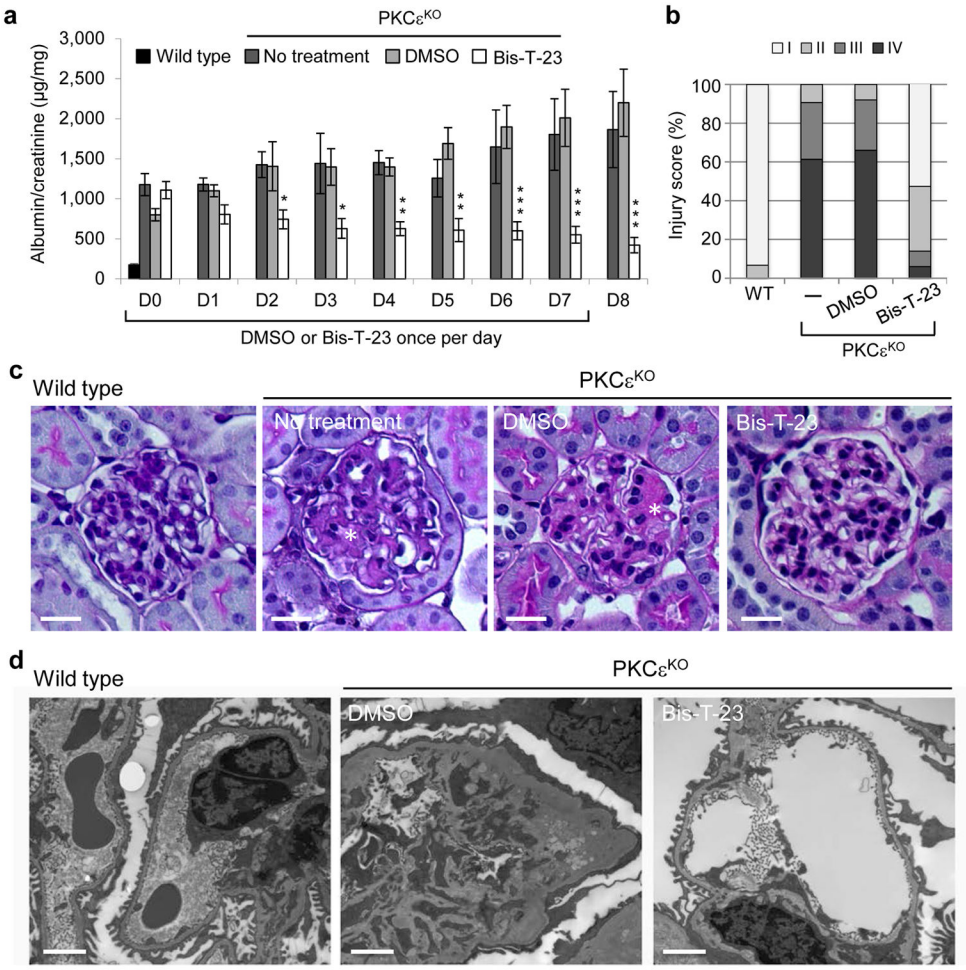

Figure 5.

Dymamin oligomerization has beneficial effect on kidney morphology in PKCε^{KO} mice. (**a**) Proteinuria in PKCε^{KO} mice without treatment or treated with either DMSO (1%, vehicle) or with Bis-T-23 (40 mg/kg) once daily for 8 consecutive days (n = 6 mice per condition) as determined by analysis of the spot urine. Animals were 12 weeks old at the beginning of the treatment (day 0, D0). Error bars, mean ± SD (*$P \leq 0.05$; **$P \leq 0.01$; ***$P \leq 0.001$; unpaired t-test). (**b**) Total of 150 glomeruli from different animals per group (n = 3) were scored in a blind manner: I = normal glomerulus, II = mild mesangial expansion, III = moderate mesangial expansion, IV = advanced mesangial matrix expansion. (**c**) Representative images of PAS-stained glomeruli (n = 150 glomeruli per condition) of 14-week-old untreated, DMSO- (1%) and Bis-T-23- (40 mg/kg) treated animals. Scale bars, 20 μm. (**d**) Representative TEM images of glomeruli (n = 10 glomeruli per group) from wild-type and PKCε^{KO} mice harvested after 8 days of injection with either DMSO (1%, vehicle) or Bis-T-23 (40 mg/kg). Scale bars, 2 μm.

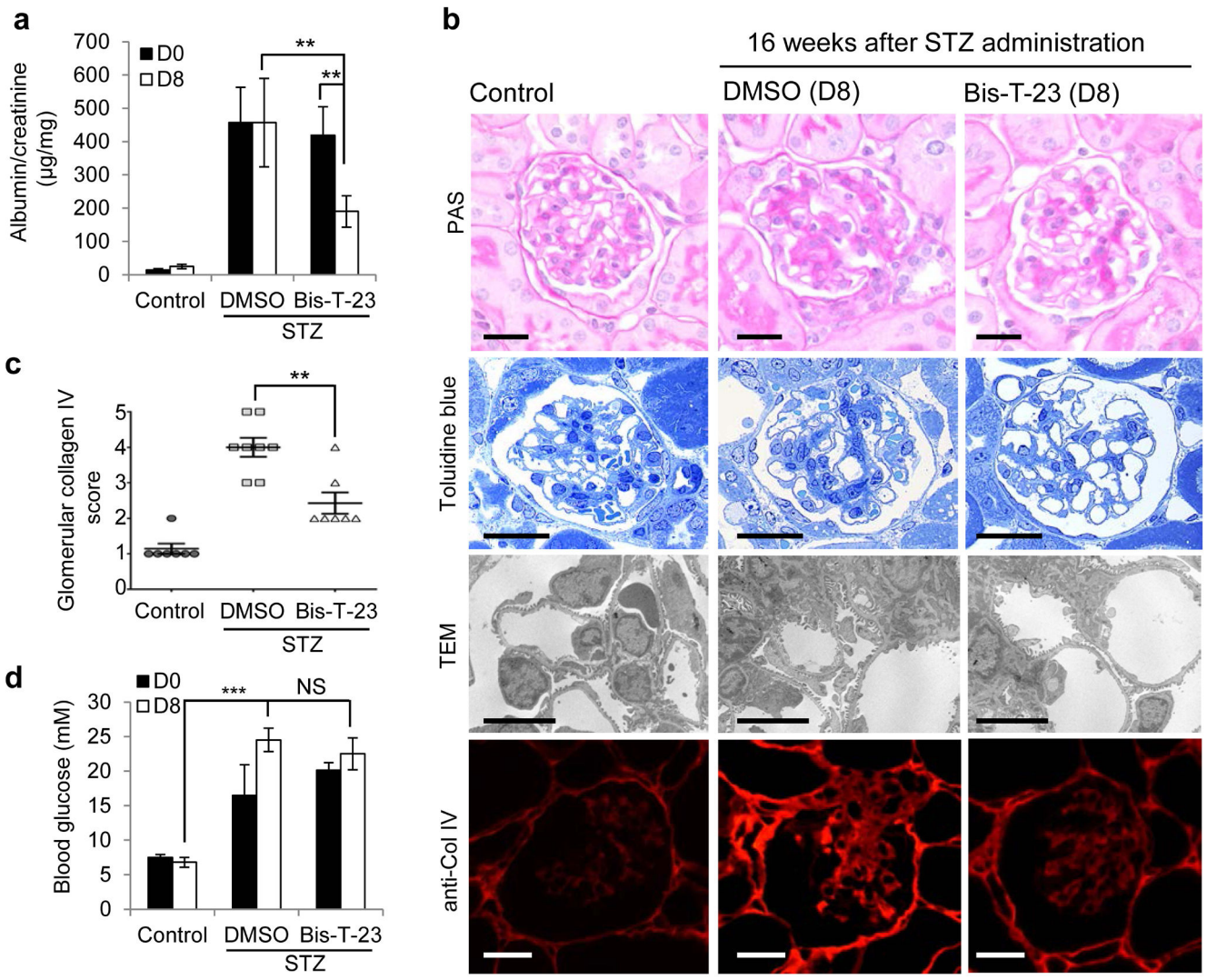

Figure 6.

Dynamin oligomerization ameliorates proteinuria due to diabetic nephropathy. (**a**) Proteinuria in 129X1/SvJ mice determined by analysis of spot urine samples after STZ-induced diabetes. Sixteen weeks after STZ injection (D0), animals were injected with either DMSO (1%, vehicle) or Bis-T-23 (20 mg/kg) once a day for 8 consecutive days (D8) (n = 8 male mice per condition). Error bars, mean ± SD (**$P \leq 0.01$; unpaired t-test). (**b**) Representative images of glomeruli stained with PAS (n = 50 glomeruli), stained with Toluidine blue (n = 15 glomeruli), by TEM (n = 15 glomeruli) and by immunofluorescence using anti-collagen IV antibody (n = 50 glomeruli). Glomeruli were isolated from control and diabetic animals treated with either DMSO (1%, vehicle) or Bis-T-23 (40 mg/kg) for 8 days, D8 in **a**. Scale bars, 20 µm (images showing PAS, Toluidine blue and collagen IV staining) and 5 µm (TEM images). (**c**) Glomerular collagen IV expression in glomeruli from the indicated mice quantified in a blind manner: 1, very mild; 2 mild; 3, moderate; 4, intense; 5 for very intense. Error bars, mean ± SD (**$P \leq 0.01$; unpaired t-test). (**d**) Blood

glucose levels in animals used in **a**. Error bars, mean ± SD. ***$P \leq 0.001$; unpaired *t*-test. NS, not statistically significant.